JHEP

Published for SISSA by Springer

Received: *March 20, 2026*
Accepted: *May 31, 2026*
Published: *July 6, 2026*

Measurement of the jet mass in hadronic decays of boosted W bosons at 13 TeV and extraction of the W boson mass

The CMS collaboration

Full author list at the end of the paper

E-mail: cms-publication-committee-chair@cern.ch

Abstract: The jet mass of W bosons decaying to a quark-antiquark pair is measured in W+jets events from proton-proton collisions at a center-of-mass energy of 13 TeV. The data used were collected by the CMS experiment at the CERN LHC and correspond to an integrated luminosity of 138 fb^{-1}. Hadronic decays of W bosons with high momenta produce strongly collimated decay products due to the large Lorentz boost, and are reconstructed as single large-radius jets. These jets have a characteristic substructure that is exploited to distinguish them from the large background of quark- and gluon-initiated jets. The jet mass is computed using the soft-drop algorithm, which suppresses soft wide-angle radiation that leads to a broadening of the jet mass distribution. For the first time, unfolded measurements are presented of the double-differential W+jets cross section as a function of the jet transverse momentum and soft-drop mass. From these distributions, the W boson mass is obtained, with a value of 80.83 ± 0.55 GeV in a scheme with mass-dependent width, achieving the smallest uncertainty available today from an all-jets final state at a hadron collider.

Keywords: Hadron-Hadron Scattering, Jets, Vector Boson Production

ArXiv ePrint: 2603.19963

https://doi.org/10.1007/JHEP07(2026)054

JHEP07(2026)054

Contents

1 Introduction **1**

2 The CMS detector and event reconstruction **3**

3 Event simulation **5**

4 Jet mass reconstruction and jet substructure tagging **6**

5 Event selection **8**

6 Background estimation **11**

7 Systematic uncertainties **13**

8 Unfolding **15**

9 Results **18**

10 Summary **23**

A Full set of reconstructed m_{SD} distributions **25**

The CMS collaboration **33**

1 Introduction

The W boson is produced at high rates in proton-proton pp collisions at the CERN LHC. The mass of the W boson, m_{W}, is among the most precisely known parameters of the standard model (SM) of particle physics, with measurements at LEP [1], Tevatron [2, 3], and LHC [4–6]. The most recent measurement by the CMS Collaboration yields $m_{\mathrm{W}} = 80.3602 \pm 0.0099\,\mathrm{GeV}$ [7], consistent with the SM expectation [8]. The large center-of-mass energy at the LHC enables the study of W bosons with very high transverse momenta $p_{\mathrm{T}} \gg m_{\mathrm{W}}$. The majority of W bosons decay into quark-antiquark pairs that appear in the detector as two separate jets. For W bosons with high p_{T} and therefore large Lorentz boosts, the quark-antiquark pair is highly collimated in the laboratory frame, such that the products of the parton showering and hadronization of the quark-antiquark pair are contained within a single large-radius jet. At the LHC, jets with high energy are produced abundantly and only a small fraction originates from W bosons. An analysis of the jet substructure can be used to identify the initiating particle of such jets. A well-established quantity to distinguish such jets from quark- and gluon-initiated background jets is the jet mass computed after the removal of soft and wide-angle radiation from the parton shower with a jet grooming technique [9, 10]. Jets initiated by boosted W bosons are the subject of many direct searches for new physics and measurements of SM properties, which are often limited by imperfect modeling of the jet substructure [11, 12]. Such modeling involves parton showering and

JHEP07(2026)054

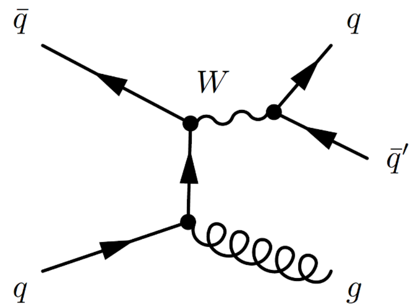

Figure 1. Example tree-level Feynman diagram contributing to $\mathrm{W}(\mathrm{q}\overline{\mathrm{q}}')$+jets production.

hadronization, described in the simulation partly by perturbative quantum chromodynamics (QCD) and partly by phenomenological models. A precise measurement and understanding of the W boson jet mass distribution is therefore important.

Previous measurements at SPS [13], LEP [1] and Tevatron [14] had extracted m_{W} using the W boson decay to a final state with a pair of jets. In this paper, we present the first measurement of the mass of large-radius jets originating from the hadronic decay of W bosons with large Lorentz boosts. We aim at improving the precision compared to previous measurements in all-jets final states at hadron colliders. The expected precision of the extracted m_{W} parameter is not yet competitive with previous measurements making use of leptonic final states. This measurement represents a first step towards a potential precision measurement of m_{W} in the all-jets final state at the high-luminosity LHC (HL-LHC) with prospects outlined in ref. [15]. The measurement reported here is mainly aimed at testing and improving the modeling of jet substructure in W boson production.

An example Feynman diagram of a boosted $\mathrm{W}(\mathrm{q}\overline{\mathrm{q}}')$+jets event is depicted in figure 1. At leading order, the jet initiated by the boosted W boson and a recoiling jet from a quark or gluon carry the same transverse momentum making them difficult to distinguish. The sample of boosted $\mathrm{W}(\mathrm{q}\overline{\mathrm{q}}')$+jets events is subject to a large background coming from multijet production through QCD processes. This introduces one of the main challenges in the analysis and is addressed with dedicated W boson jet tagging approaches for background removal and an estimate of the remaining QCD multijet background using control samples in data. Ordinary QCD jets acquire mass from splittings of quarks and gluons in the parton shower. To mitigate the effects of soft and wide-angle radiation that obscure the jet mass, the modified mass drop algorithm [16, 17], which is a specific example of soft-drop (SD) grooming [18], is applied. This technique removes soft and wide-angle radiation below a specified threshold. Applying grooming significantly reduces the mass of quark- and gluon-initiated jets, while bringing the mass of signal jets closer to the W boson mass, thereby enhancing the signal-to-background ratio for W boson identification. In addition, events are categorized using a jet substructure tagger that distinguishes the characteristic 'two-prong' substructure, corresponding to the fragmentation and hadronization of the two colored partons from the W boson decay, from the 'one-prong' background, where prongs are localized clusters of energy within the collection of final-state particles of the jet.

The analysis uses pp collision data at $\sqrt{s} = 13\,\mathrm{TeV}$ recorded by the CMS experiment [19] at the LHC during 2016–2018, corresponding to an integrated luminosity of $138\,\mathrm{fb}^{-1}$. Measurements of the jet mass distribution have been previously performed at the LHC for light-quark and gluon jets [20–22], top quark jets [23–25], and Z boson jets [26]. The measurements of quark and gluon jets offer a testbed for perturbative and nonperturbative QCD predictions. The study of the top quark jet mass enables the determination of the top quark mass using a sample of boosted W bosons for the jet mass calibration, which relies on a precise understanding of jet substructure in events with a color-connected top quark-antiquark pair ($\mathrm{t\bar{t}}$). The $\mathrm{W(q\bar{q}')}$+jets process offers a sample of boosted W bosons decaying to a quark-antiquark pair that is not color-connected to the remainder of the event. In this paper, the groomed jet mass distribution of $\mathrm{W(q\bar{q}')}$+jets events is measured in intervals of the jet transverse momentum with $p_{\mathrm{T}} > 650\,\mathrm{GeV}$. A two-dimensional unfolding of the data in jet mass and p_{T} is performed using a maximum-likelihood template fit. Finally, m_{W} is extracted using a template fit to the unfolded data.

The paper is organized as follows. In section 2 a brief description of the CMS detector and event reconstruction is given. Section 3 provides details on the simulation used for the analysis. The jet mass observable and jet substructure algorithms are explained in section 4. This is followed by descriptions of the event selection in section 5, the background estimation procedure in section 6 and the uncertainties in section 7. The unfolding of the data for detector effects is described in section 8 and the results of the cross section measurement and the estimation of the m_{W} parameter are presented in section 9. Section 10 summarizes the paper.

2 The CMS detector and event reconstruction

The central feature of the CMS apparatus [19, 27] is a superconducting solenoid of 6 m internal diameter, providing a magnetic field of 3.8 T. Within the solenoid volume are a silicon pixel and strip tracker, a lead tungstate crystal electromagnetic calorimeter (ECAL), and a brass and scintillator hadron calorimeter (HCAL), each composed of a barrel and two endcap sections. Forward calorimeters extend the pseudorapidity (η) coverage provided by the barrel and endcap detectors. Muons are detected in gas-ionization chambers embedded in the steel flux-return yoke outside the solenoid. A more detailed description of the CMS detector, together with a definition of the coordinate system used and the relevant kinematic variables, can be found in refs. [19, 27].

The silicon tracker used in 2016 measured charged particles within the range $|\eta| < 2.5$. For nonisolated particles of $1 < p_{\mathrm{T}} < 10\,\mathrm{GeV}$ and $|\eta| < 1.4$, the track resolutions were typically 1.5% in p_{T} and 25–90 (45–150) μm in the transverse (longitudinal) impact parameter [28]. At the start of 2017, a new pixel detector was installed [29]; the upgraded tracker measured particles up to $|\eta| = 3.0$ with typical resolutions of 1.5% in p_{T} and 20–75 μm in the transverse impact parameter [30] for nonisolated particles of $1 < p_{\mathrm{T}} < 10\,\mathrm{GeV}$. According to simulation studies [31], similar improvements are expected in the longitudinal direction.

Events of interest are selected using a two-tiered trigger system. The first level, composed of custom hardware processors, uses information from the calorimeters and muon detectors to select events at a rate of around 100 kHz within a fixed latency of 4 μs [32]. The second level, known as the high-level trigger, consists of a farm of processors running a version of the full event reconstruction software optimized for fast processing, and reduces the event rate to a few kHz before data storage [33, 34].

JHEP07(2026)054

The particle-flow (PF) algorithm [35] aims to reconstruct and identify each individual particle in an event, with an optimized combination of information from the various elements of the CMS detector. The energy of photons is obtained from the ECAL measurement. The energy of electrons is determined from a combination of the electron momentum at the primary interaction vertex as determined by the tracker, the energy of the corresponding ECAL cluster, and the energy sum of all bremsstrahlung photons spatially compatible with originating from the electron track. The energy of muons is obtained from the curvature of the corresponding track. The energy of charged hadrons is determined from a combination of their momentum measured in the tracker and the matching ECAL and HCAL energy deposits, corrected for the response function of the calorimeters to hadronic showers. Finally, the energy of neutral hadrons is obtained from the corrected ECAL and HCAL energies.

The primary vertex (PV) is taken to be the vertex corresponding to the hardest scattering in the event, evaluated using tracking information alone, as described in section 9.4.1 of ref. [36]. Additional pp interactions within the same or nearby bunch crossings (pileup) can contribute additional tracks and calorimetric energy depositions to the jet momentum [37]. The pileup per particle identification algorithm (PUPPI) [38, 39] is used to mitigate the effect of pileup at the reconstructed particle level, making use of local shape information, event pileup properties, and tracking information. A local shape variable is defined, which distinguishes between collinear and soft diffuse distributions of other particles surrounding the particle under consideration. The former is attributed to particles originating from the PV and the latter to particles originating from pileup interactions. Charged particles identified to be originating from pileup vertices are discarded. For each neutral particle, a local shape variable is computed using the surrounding charged particles compatible with the PV within the tracker acceptance ($|\eta| < 2.5$), and using both charged and neutral particles in the region outside of the tracker coverage. The momenta of the neutral particles are then rescaled according to their probability to originate from the PV, deduced from the local shape variable, superseding the need for jet-based pileup corrections [38].

For each event, hadronic jets are clustered from the reconstructed PF candidates with the PUPPI weights applied, using the infrared and collinear safe anti-k_{T} algorithm [40, 41] with a distance parameter $R = 0.8$. The jet momentum is determined as the vectorial sum of all particle momenta in the jet. It is found from simulation to be, on average, within 5 to 10% of the true momentum over the entire p_{T} spectrum and detector acceptance. Jet energy corrections are derived from simulation to adjust the measured response of jets to that of particle-level jets on average. In-situ measurements of the momentum balance in dijet, γ+jets, Z+jets, and multijet events are used to account for any residual differences in jet energy scale in experimental data and simulation [42]. The jet energy resolution amounts typically to 15% at 10 GeV, 8% at 100 GeV, and 4% at 1 TeV. Additional selection criteria are applied to each jet to remove jets potentially dominated by instrumental effects or reconstruction failures [38].

In simulation, we also cluster particle-level jets using the same jet algorithm from final-state particles with proper lifetime $c\tau > 10\,\mathrm{mm}$, after hadronization, where c is the speed of light. The distance parameter is $R = 0.8$ unless quoted otherwise.

The techniques used for the reconstruction of the jet mass and jet substructure are discussed in section 4.

JHEP07(2026)054

3 Event simulation

The simulation of pp collision events is performed using various software packages in multiple steps. Processes of $\mathrm{W(q\overline{q}')}$+jets, and $\mathrm{Z(q\overline{q})}$+jets are generated at leading order (LO) using MadGraph5_aMC@NLO v2.6.5 [43] with additional partons added to the matrix element computation. The $\mathrm{W(q\overline{q}')}$+jets sample is generated with up to three additional partons, while the $\mathrm{Z(q\overline{q})}$+jets one is generated with up to four partons. The MadGraph5_aMC@NLO generator is interfaced to pythia 8.309 [44] with the CP5 tune [45] for the parton showering and hadronization. pythia implements a dipole shower ordered in p_{T} and the hadronization of quarks and gluons into final hadrons is described by the Lund string model [46, 47]. To avoid double-counting of jets from the matrix element calculations and the parton shower, jets are matched using the MLM scheme [48]. An alternative sample of $\mathrm{W(q\overline{q}')}$+jets is obtained interfacing MadGraph5_aMC@NLO with herwig 7.2.2 [49] at LO with angular-ordered showering and the CH3 tune [50]. The sample is generated with up to three jets in the final state using FxFx matching [51]. The MadGraph5_aMC@NLO generator is used to generate samples of QCD multijet events binned in the scalar sum of all jet transverse momenta (H_{T}) at LO with up to four $R = 0.4$ jets in the final state that are showered with pythia using MLM matching. The powheg v2 generator [52–54] is used for the simulation of the $\mathrm{t\overline{t}}$ process at next-to-LO (NLO) accuracy in perturbative QCD [55] and is interfaced with pythia. All samples are generated using the NNPDF3.1 [56] parton distribution function (PDF) sets at next-to-NLO (NNLO) accuracy. The generated events are then passed through the Geant4 [57] package to simulate the CMS detector response before they are treated with the same reconstruction algorithms as the real data.

The simulated events are corrected for various effects, which are not well modeled in the simulation. These correction factors are applied to the simulated events as event weights. The $\mathrm{W(q\overline{q}')}$+jets and $\mathrm{Z(q\overline{q})}$+jets samples are corrected to higher-order precision using the same dedicated correction factors as derived in ref. [58]. These corrections are multiplicative factors for the differential cross section of the V+jets (where V stands for W or Z) processes as a function of the p_{T} of the vector boson. They include higher-order QCD and electroweak (EW) effects. The QCD corrections were derived from NLO V+jets samples generated using MadGraph5_aMC@NLO, whereas the EW corrections are based on higher-order calculations at NLO EW precision [59]. The NLO powheg+pythia $\mathrm{t\overline{t}}$ samples used in the analysis show deviations in the p_{T} spectrum of top quarks when compared to data [60, 61]. We apply a reweighting of $\mathrm{t\overline{t}}$ events based on the measurements of the top quark p_{T}.

As the detector conditions have varied throughout the data taking, four separate sets of simulations with corresponding correction factors matching four data-taking periods (early 2016, late 2016, 2017, and 2018) are used. The events are generated with a distribution in the number of pileup interactions per proton bunch crossing, which is not the same as in observed events. All simulated events are reweighted to match the profile of that in the respective data-taking period.

JHEP07(2026)054

4 Jet mass reconstruction and jet substructure tagging

The jet with the largest p_{T} in the event, referred to as the leading jet, is considered the boosted W boson candidate. While at leading order, the chance of selecting a jet from the recoiling quark or gluon in a $\mathrm{W(q\overline{q}')}$+jets event rather than the boosted W boson is 50%, this fraction is strongly reduced by further selections on jet substructure as explained in the following.

The constituents of the leading jet are reclustered with the Cambridge-Aachen (CA) algorithm [62], and then groomed using the SD algorithm. The SD algorithm splits the jet into two subjets when undoing the last step of the CA jet clustering. It is then checked if the two subjets satisfy the condition

$$\frac{\min(p_{\mathrm{T}}^{(1)}, p_{\mathrm{T}}^{(2)})}{p_{\mathrm{T}}^{(1)} + p_{\mathrm{T}}^{(2)}} > z_{\mathrm{cut}} \left(\frac{\Delta R_{12}}{R}\right)^{\beta_{\mathrm{sd}}}, \qquad (4.1)$$

where $p_{\mathrm{T}}^{(1)}$ and $p_{\mathrm{T}}^{(2)}$ are the transverse momenta of the two subjets, R is the jet radius parameter, $\Delta R_{12} = \sqrt{(\Delta y_{12})^2 + (\Delta\phi_{12})^2}$ is the distance between the two subjets with the rapidity and azimuthal differences Δy_{12} and $\Delta\phi_{12}$, and z_{cut} and β_{sd} are tunable parameters of the SD algorithm, set to default parameters $z_{\mathrm{cut}} = 0.1$ and $\beta_{\mathrm{sd}} = 0$ used in CMS studies [63]. In ref. [15], it was shown that the SD algorithm with this set of parameters is well suited for this measurement in combination with a jet substructure tagger to reduce sensitivity to nonperturbative effects. If the condition is met, the vectorial sum of the two subjets is returned as the SD groomed jet. If the condition is not met, the subjet with the lower p_{T} is rejected. The declustering procedure is then repeated by splitting the higher-p_{T} subjet into two subjets, undoing another CA clustering step, and iterating until the condition is met. This grooming procedure removes soft and wide-angle radiation from the jet, thereby making the jet mass more resilient to effects from pileup, underlying event, and initial-state radiation. The jet p_{T} used for the measurement is taken from the original ungroomed anti-k_{T} jet, because anti-k_{T} jet p_{T} is resistant to soft and wide-angle radiation. The SD grooming is only applied to compute the jet mass.

The reconstructed SD jet mass, m_{SD}, is corrected to match that of particle-level jets on average in two steps. First, jet energy corrections [42] are applied to the momenta of the SD subjets of the uncalibrated CA jets, matching the response in data to that of particle-level jets. As the m_{SD} is strongly correlated with the momenta of the subjets, this procedure yields a reconstructed m_{SD} in data close to the particle-level SD jet mass $m_{\mathrm{SD}}^{\mathrm{ptcl}}$. Second, we apply p_{T}-dependent corrections of 2–6%, derived from the ratio of the reconstructed SD jet mass to the particle-level SD jet mass in simulated $\mathrm{W(q\overline{q}')}$+jets events. While this correction does not modify the data-to-simulation agreement, it simplifies the unfolding by yielding a response closer to unity. Because of the PUPPI algorithm, the jet m_{SD} is almost insensitive to pileup [38]. It should be noted that this procedure does not rely on data samples containing boosted W bosons, but rather independent dijet, γ+jets, Z+jets, and multijet data samples for calibration, in order to avoid any bias to the mass measurement.

We use jet substructure taggers that distinguish the characteristic two-prong substructure of jets from boosted W bosons from light-flavor quark and gluon background jets. We carry out the analysis with two different tagging strategies, first with a well-established

JHEP07(2026)054

jet substructure observable $N_2^{(1)}$ [64, 65] and second with a neural-network classifier called ParticleNet [66]. The $N_2^{(1)}$-based tagger is closer to a theoretically well-defined particle-level observable, thus it can yield smaller extrapolation uncertainties between detector and particle levels. The ParticleNet tagger provides a cleaner sample with less background, thus it can yield smaller experimental uncertainties. Whereas for a future measurement with a larger data set, e.g. at the HL-LHC, the $N_2^{(1)}$-based approach may be more suitable, for this measurement, the ParticleNet approach is presented as the main result, and the $N_2^{(1)}$-based approach as a cross-check.

The $N_2^{(1)}$ observable is a combination of energy correlation functions (ECFs) [64, 65]

$$ {}_{\nu}e_n^{(\beta)} = \sum_{1\leq i_1 \leq i_2 < \cdots < i_n \leq n_J} \left(\prod_{a=1}^{n} z_{i_a} \right) \prod_{m=1}^{\nu} \min_{s<t\in i_1, i_2, \ldots, i_n}^{(m)} (\Delta R_{s,t})^{\beta} , \tag{4.2} $$

with the energy fractions $z_i = \frac{p_{\mathrm{T},i}}{p_{\mathrm{T},J}}$, the particle and jet transverse momenta $p_{\mathrm{T},i}$ and $p_{\mathrm{T},J}$, the number of constituent particles n_J in the jet, the number of particles to correlate n, the chosen number ν of angles $\Delta R_{s,t}$ between particles with indices s and t entering the product, and the angular exponent β. The N_i series of ECF ratios is designed to distinguish jets with N-prong substructure,

$$ N_n^{(\beta)} = \frac{{}_2e_{n+1}^{(\beta)}}{\left({}_1e_n^{(\beta)}\right)^2}. \tag{4.3} $$

In the context of this paper, the variable $N_2^{(1)}$ is used for the identification of W boson jets. Using the definition of generalized ECFs in eq. (4.2) with $\beta = 1$, the variable $N_2^{(1)}$ is defined using the following two-point and three-point correlation functions:

$$ \begin{aligned} {}_2e_3^{(1)} &= \sum_{1\leq i\leq j\leq k\leq n_J} z_i z_j z_k \min\left\{\Delta R_{ij}\Delta R_{ik}, \Delta R_{ij}\Delta R_{jk}, \Delta R_{ik}\Delta R_{jk}\right\} , \\ {}_1e_2^{(1)} &= \sum_{1\leq i\leq j\leq n_J} z_i z_j \Delta R_{ij}. \end{aligned} \tag{4.4} $$

The ParticleNet [66] algorithm is a graph neural network (GNN) based on a dynamic graph convolutional neural network [67], designed to discriminate hadronic decays of highly boosted top quarks, W, Z, and Higgs bosons from QCD multijet background. Whereas many other machine-learning approaches treat the jet as an ordered structure [63], the ParticleNet algorithm treats jets as particle clouds, i.e., an unordered, permutation-invariant set of particles. The GNN yields probability scores (in the following called P^{PN}) for each class of process used in the training. Each class corresponds to a decay mode of the considered particle-category (e.g., $\mathrm{W} \to \mathrm{q}\overline{\mathrm{q}}'$, where $\mathrm{q} \in [\mathrm{u}, \mathrm{d}, \mathrm{s}]$). The ParticleNet algorithm is trained with the jet constituents (PUPPI weighted PF candidates) and secondary vertices associated with the jet. Input for each particle is information about its kinematic properties (p_{T}, η, ϕ, energy), its charge, and the difference of each kinematic property and the corresponding property of the jet. The secondary vertices include information about their kinematics, displacement, and quality criteria. The $P^{\mathrm{PN}}_{\mathrm{Wvs.\ QCD}}$ discriminator is defined as the ratio of the sum of probability scores of the GNN for $\mathrm{W} \to \mathrm{q}\overline{\mathrm{q}}'$, where $\mathrm{q} \in [\mathrm{u}, \mathrm{d}, \mathrm{s}, \mathrm{c}]$, and the sum over the $\mathrm{W} \to \mathrm{q\overline{q}'}$ and QCD multijet background modes includes all decay modes considered by ParticleNet.

The $N_2^{(1)}$ observable and the ParticleNet discriminator are correlated with m_{SD}. In this measurement, a technique to estimate the QCD multijet background described in section 6 relies on a mass-decorrelated tagging variable for the construction of the control region (CR) and signal region (SR). We therefore construct mass-decorrelated versions of the $N_2^{(1)}$ and ParticleNet discriminants. For ParticleNet, the GNN architecture is trained using a signal sample that consists of a generic spin-0 particle X with a uniform mass distribution that decays into two highly Lorentz-boosted particles. This dedicated mass-decorrelated (MD) training is referred to as ParticleNet-MD. Additionally, the jets used in the training are reweighted both in the signal and in the QCD background sample to have a flat jet p_{T} and m_{SD} spectrum [68]. Finally, for both $N_2^{(1)}$ and ParticleNet-MD, we follow the design decorrelated tagger (DDT) [69, 70] approach to modify the tagging variables. This approach decorrelates the tagging variable by enforcing a constant selection efficiency for QCD multijet background jets across the probed phase space. The DDT approach introduces the variable $\rho_{\mathrm{SD}} = 2\ln(\frac{m_{\mathrm{SD}}}{p_{\mathrm{T}}})$ [16], whose distribution is approximately independent of p_{T} for QCD jets. Whereas m_{SD} and p_{T} could be used interchangeably for ρ_{SD} and p_{T}, the latter allow to describe the phase space more conveniently for QCD jets. Here, the approach pioneered by CMS [70] is adopted, thus the decorrelation is flattening the $(\rho_{\mathrm{SD}}, p_{\mathrm{T}})$-dependence of the tagging variable. For this, a constant selection efficiency for QCD jets across the $(\rho_{\mathrm{SD}}, p_{\mathrm{T}})$ plane is enforced when selecting on $N_2^{(1)}$ or $P^{\mathrm{PN}}_{\mathrm{Wvs.\ QCD}}$. The decorrelated variables $N_2^{(1),\mathrm{DDT}}$ and $P^{\mathrm{PN,DDT}}_{\mathrm{Wvs.\ QCD}}$, where the latter is also referred to as ParticleNet$^{\mathrm{DDT}}$, are defined as

$$\begin{aligned} N_2^{(1),\mathrm{DDT}} &= N_2^{(1)} - P^X_{N_2^{(1)}}(\rho_{\mathrm{SD}}, p_{\mathrm{T}}), \\ P^{\mathrm{PN,DDT}}_{\mathrm{Wvs.\ QCD}} &= P^X_{P^{\mathrm{PN}}_{\mathrm{Wvs.\ QCD}}}(\rho_{\mathrm{SD}}, p_{\mathrm{T}}) - P^{\mathrm{PN}}_{\mathrm{Wvs.\ QCD}}, \end{aligned} \tag{4.5}$$

where P_i^X denotes the X-th QCD selection efficiency percentile of the tagger i as a function of ρ_{SD} and p_{T}. The two taggers are then used by requiring the new variables to be negative, i.e., $N_2^{(1),\mathrm{DDT}} < 0$ and $P^{\mathrm{PN,DDT}}_{\mathrm{Wvs.\ QCD}} < 0$ to identify W jets.

5 Event selection

The data were collected by the CMS experiment in the years 2016–2018 and correspond to an integrated luminosity of $138\,\mathrm{fb}^{-1}$. Triggers requiring an anti-k_{T} jet with $R = 0.8$ and a minimum p_{T} of 450 and 500 GeV are used to collect $\mathrm{W(q\overline{q}')}$+jets events. The trigger with $p_{\mathrm{T}} > 450\,\mathrm{GeV}$ was prescaled during part of the data taking, resulting in a lower effective luminosity of $56.6\,\mathrm{fb}^{-1}$. The trigger with $p_{\mathrm{T}} > 500\,\mathrm{GeV}$ was unprescaled, but inactive during a small fraction of data taking. The data collected with this trigger correspond to an integrated luminosity of $135\,\mathrm{fb}^{-1}$. The two triggers are used to select event samples with offline jets passing $575 < p_{\mathrm{T}} < 650\,\mathrm{GeV}$ and $p_{\mathrm{T}} > 650\,\mathrm{GeV}$, respectively. Both triggers are more than 99.9% efficient. To account for residual differences in trigger efficiency in data and the modeled efficiency in the simulation, data-to-simulation scale factors are measured and applied as event weights to the simulation.

	$N_2^{(1),\mathrm{DDT}}$		$P^{\mathrm{PN,DDT}}_{\mathrm{Wvs.\ QCD}}$	
	$\varepsilon_{\mathrm{W+jets}}$	$\varepsilon_{\mathrm{bkg}}$	$\varepsilon_{\mathrm{W+jets}}$	$\varepsilon_{\mathrm{bkg}}$
Pass	18.5%	4.1%	38.2%	4.2%
Fail	81.5%	95.9%	61.8%	95.8%

Table 1. Summary of signal ($\varepsilon_{\mathrm{W+jets}}$) and background ($\varepsilon_{\mathrm{bkg}}$) efficiencies in the different signal (pass) and control (fail) regions for the $N_2^{(1),\mathrm{DDT}}$ and $P^{\mathrm{PN,DDT}}_{\mathrm{Wvs.\ QCD}}$ taggers in the fully-hadronic $\mathrm{W}(\mathrm{q\overline{q}'})$+jets selection. The efficiencies are estimated from simulation and averaged over the years of data-taking.

After reconstruction and calibration, events are required to have at least one jet with $p_{\mathrm{T}} > 575\,\mathrm{GeV}$ and $|\eta| < 2.4$. The measurement is carried out in p_{T} intervals (bins) with the low bin edges at 575, 650, 725, 800, 1000, 1200 GeV, and larger (denoted by ∞). This choice of bin edges ensures that the bin width is well above the experimental resolution of the order 5–10% and the number of bins is small enough to have reasonable statistical uncertainties in all bins. Additional selection criteria are applied to remove jets potentially dominated by anomalous contributions from various subdetector components or reconstruction failures [38]. In 2018, two sectors of the HCAL endcap in the region $-1.57 < \phi < -0.87$ and $-3.2 < \eta < -1.3$ were not functional for the last $\approx$65% of the data taking. In data recorded during this time, events are rejected if the leading jet is reconstructed within this region. Events in the simulation are weighted accordingly if the leading jet is reconstructed in this region to reflect the resulting inefficiency. Events with a reconstructed electron or muon with $p_{\mathrm{T}} > 10\,\mathrm{GeV}$ and $|\eta| < 2.4$ and passing loose identification criteria [37, 71] are rejected to suppress backgrounds with lepton final states.

The main backgrounds of the measurement are processes with high-p_{T} quark and gluon jets, which arise from QCD multijet processes or $\mathrm{W}(\mathrm{q\overline{q}'})$+jets events where the leading jet is not initiated by the W boson decay, but rather by a recoiling quark or gluon. At LO, the jet initiated by the boosted W boson and the recoiling jet from a quark or gluon carry opposite transverse momentum, while at higher orders, the W boson jet is more likely to be reconstructed as the leading jet. Two handles to suppress those backgrounds are first the m_{SD} and second jet substructure taggers that distinguish the characteristic two-prong substructure of boosted W boson jets from background.

The leading jet is required to have $m_{\mathrm{SD}} > 50\,\mathrm{GeV}$ to reject background from quark and gluon jets. Further, the jet is required to have $\rho_{\mathrm{SD}} < -2.1$ to reject events with high m_{SD} but low jet p_{T} and avoid instabilities and edge effects from the SD algorithm and jet clustering [72]. For jets from boosted W bosons this selection ensures that the decay products of the W boson are fully merged within a jet with $R = 0.8$.

Events are finally categorized into signal (pass) and control (fail) regions using a mass-decorrelated jet substructure tagger with a QCD background efficiency of 5%. The corresponding signal and background efficiencies for both tagging approaches are summarized in table 1. The $P^{\mathrm{PN,DDT}}_{\mathrm{Wvs.\ QCD}}$ approach yields a significantly larger signal efficiency at a similar background efficiency.

In this measurement, we carry out an unfolding of the data to the particle level (ptcl). At the particle level, we require at least one anti-k_{T} jet with $R = 0.8$ and with $p_{\mathrm{T}}^{\mathrm{ptcl}} > 500\,\mathrm{GeV}$

Selection	Cross section [fb]
$p_{\mathrm{T}}^{\mathrm{ptcl}} > 650\,\mathrm{GeV}$	1396^{+116}_{-146}
$p_{\mathrm{T}}^{\mathrm{ptcl}} > 650\,\mathrm{GeV}$ & $m_{\mathrm{SD}}^{\mathrm{ptcl}} > 30\,\mathrm{GeV}$	888^{+74}_{-93}
$p_{\mathrm{T}}^{\mathrm{ptcl}} > 650\,\mathrm{GeV}$ & $m_{\mathrm{SD}}^{\mathrm{ptcl}} > 30\,\mathrm{GeV}$ & $N_2^{(1)} < 0.2$	241^{+24}_{-21}

Table 2. Fiducial $\mathrm{W(q\overline{q}')}$+jets cross sections predicted by MadGraph5_aMC@NLO+PYTHIA at NLO QCD with EW corrections after different stages of the particle-level selection. The given uncertainty is the sum in quadrature of parton shower variations and the hadronization model uncertainty, as well as the uncertainties in the QCD and EW corrections.

JHEP07(2026)054

and $m_{\mathrm{SD}}^{\mathrm{ptcl}} > 30\,\mathrm{GeV}$. The measurement is carried out in $p_{\mathrm{T}}^{\mathrm{ptcl}}$ and $m_{\mathrm{SD}}^{\mathrm{ptcl}}$ bins with lower bin edges at 500, 650, 800 and 1200 GeV, and 30, 70, 80 and 90 GeV, respectively. While the $500 < p_{\mathrm{T}}^{\mathrm{ptcl}} < 650\,\mathrm{GeV}$ bin is taken into account in the migration matrix, the final result is presented for $p_{\mathrm{T}}^{\mathrm{ptcl}} > 650\,\mathrm{GeV}$. The binning of $p_{\mathrm{T}}^{\mathrm{ptcl}}$ is chosen to have twice the bin width of the binning at the detector level, which is a typical choice when using a maximum likelihood fit based unfolding. The approach requires having more bins at the detector level than at the particle level to have an over-constrained fit. The binning of $m_{\mathrm{SD}}^{\mathrm{ptcl}}$ is chosen such that the stability and purity are above approximately 50% for all bins. The stability is the fraction of events in a given bin at the particle level that are reconstructed in the same bin at the detector level. Similarly, purity is the fraction of events that are reconstructed in a given bin at the detector level and originate from the same bin at the particle level. At detector level, a finer binning in steps of 5 GeV in m_{SD} is chosen to offer more constraining power to the background estimation procedure. In addition, we require $N_2^{(1)} < 0.2$ at the particle level. The corresponding fiducial cross sections at each stage of the particle-level selection are reported in table 2, computed with MadGraph5_aMC@NLO+PYTHIA at NLO QCD and with EW corrections.

Figure 2 shows the acceptance of the detector-level selection, which includes the jet p_{T}, $|\eta|$, and m_{SD} requirements and a matching within $\Delta R < 0.4$ between the detector-level jet and the particle-level jet corresponding to the simulated W boson. The first and last bins in $m_{\mathrm{SD}}^{\mathrm{ptcl}}$ have a low acceptance of 5–20%, especially in the first and last $p_{\mathrm{T}}^{\mathrm{ptcl}}$ bins, mainly because the selected detector-level jet often does not match to the simulated W boson, when outside the W boson peak region. The central $m_{\mathrm{SD}}^{\mathrm{ptcl}}$ bins in the W boson mass peak region have a much larger acceptance of 30–70%. When including the $N_2^{(1)} < 0.2$ selection in the particle-level definition, the acceptance is significantly larger. The efficiencies of the trigger and jet reconstruction are larger than 99% and accounted for as well.

In figure 3, examples of the reconstructed m_{SD} distributions in signal and control regions are shown for the second p_{T} bin after the background estimation and a fit to the data distribution, discussed in section 6. The full set of reconstructed m_{SD} distributions can be found in appendix A, figure 10–12. The dominant background in both SR and CR is from QCD multijet production that follows a smoothly falling distribution. The signal $\mathrm{W(q\overline{q}')}$+jets events and backgrounds from $\mathrm{Z(q\overline{q})}$+jets and $\mathrm{t\overline{t}}$ exhibit peaks at the respective W, Z, and t quark masses in the SR, while they contribute negligibly to the CR. The peaks are more pronounced in the SR obtained with the $P_{\mathrm{W vs.\,QCD}}^{\mathrm{PN,DDT}}$ tagger compared to the $N_2^{(1),\mathrm{DDT}}$ tagger,

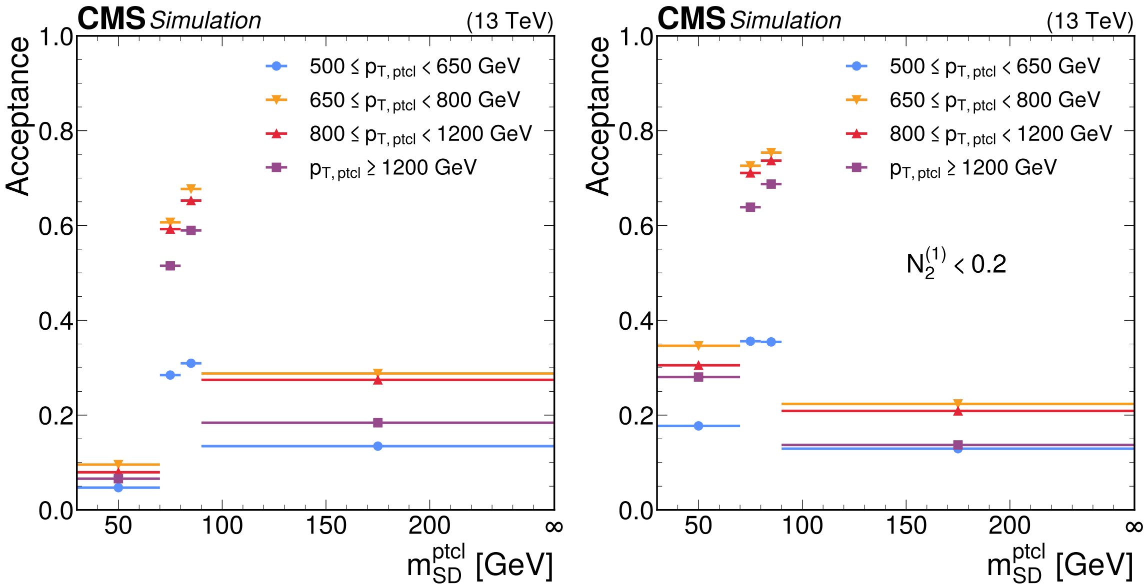

Figure 2. Acceptance as a function of $m_{\mathrm{SD}}^{\mathrm{ptcl}}$ without (left) and with (right) the requirement $N_2^{(1)} < 0.2$ at the particle level. The acceptance is calculated using the $\mathrm{W}(\mathrm{q\overline{q}}')$+jets signal simulation with 2018 detector conditions.

due to the higher efficiency. The detector-level jets from the $\mathrm{W}(\mathrm{q\overline{q}}')$+jets simulation are matched to particle-level jets. The corresponding distributions are labeled "merged W", while jets not matched to the generated W boson are labeled "not merged".

For the statistical analysis of the data and estimation of the background, a maximum likelihood template fit is performed using histograms of m_{SD} in the SR and CR. The construction of the likelihood functions and the minimization of the negative log-likelihood is performed using the COMBINE toolkit [73].

6 Background estimation

After the event selection, the data sample is dominated by QCD multijet events, which are difficult to model in simulation. Therefore, an approach based on control samples of observed events is used to estimate the QCD multijet background, while the remaining processes are estimated from simulation. This approach is based on an established method as used in previous CMS analyses [58, 70]. The method is based on the assumption that the shape of the m_{SD} distribution in QCD multijet events is similar in the pass and fail regions of a given substructure tagger that has been decorrelated with m_{SD}. Consequently, one can estimate the shape of the QCD background from the signal-depleted fail region from data, and use a transfer factor to extrapolate the shape to the signal-enriched pass region. Ideally, this transfer factor is a constant, equal to the selection efficiency $\varepsilon_{\mathrm{QCD}}$ measured in a QCD multijet sample. If the data were perfectly described by simulation, the efficiency $\varepsilon_{\mathrm{QCD}}$ could be obtained from simulated QCD multijet events since a pure background sample is impossible to obtain from data. However, the jet tagging efficiency is not perfectly modeled in simulation and is not a constant, but depends on the jet kinematics, primarily on the jet p_{T}.

JHEP07(2026)054

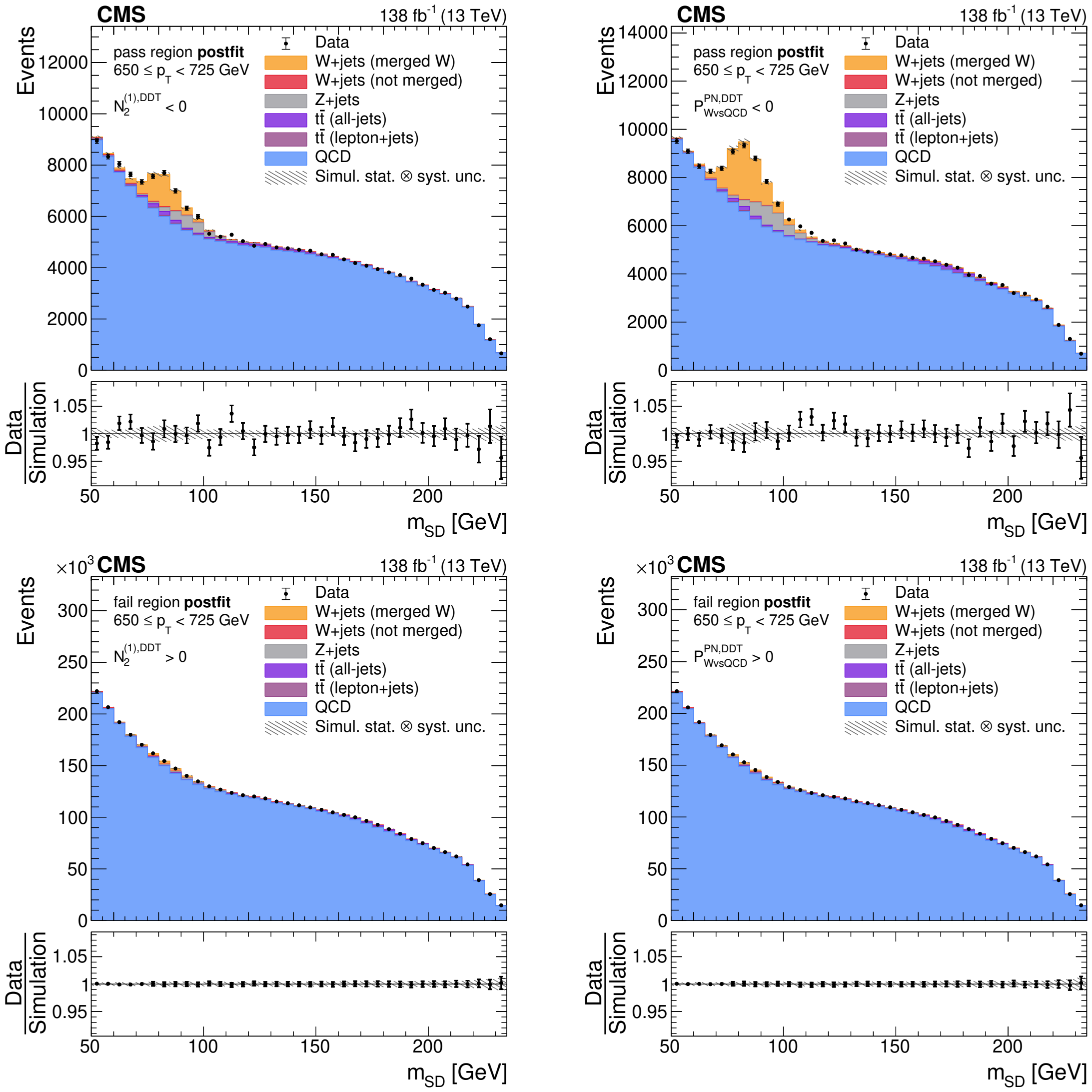

Figure 3. Reconstructed m_{SD} distributions in the second p_{T} bin with $650 < p_{\mathrm{T}} < 725\,\mathrm{GeV}$ in the signal (upper row) and control (lower row) regions defined using the $N_2^{(1),\mathrm{DDT}}$ (left) and $P^{\mathrm{PN,DDT}}_{\mathrm{Wvs.\ QCD}}$ (right) taggers after the background estimation and a fit to the data, explained in section 6. All four data-taking periods are combined, resulting in a total integrated luminosity of 138 fb^{-1}. The lower panels show the data-to-simulation ratio. The error bars correspond to the statistical uncertainty in the data. The dashed band is the total uncertainty on the background after a fit to the data distribution.

Additionally, the jet tagging variables are not entirely decorrelated with m_{SD}, despite efforts to explicitly decorrelate them as described above. We address this by using a two-dimensional transfer function that depends on p_{T} and ρ_{SD} of the jet,

$$\mathrm{TF}(\hat{p}_{\mathrm{T}}, \hat{\rho}_{\mathrm{SD}}) = \varepsilon_{QCD}(\hat{p}_{\mathrm{T}})\, r(\hat{p}_{\mathrm{T}}, \hat{\rho}_{\mathrm{SD}}), \tag{6.1}$$

where $\hat{p}_{\mathrm{T}}$ and $\hat{\rho}_{\mathrm{SD}}$ are functions of m_{SD} and p_{T} and correspond to the normalized observables p_{T} and ρ_{SD}, scaled to lie in the interval $[0, 1]$. The efficiency $\varepsilon_{QCD}(\hat{p}_{\mathrm{T}})$ is obtained from simulated QCD multijet events, separately for each data-taking period. The residual function

JHEP07(2026)054

$r(\hat{p}_\mathrm{T}, \hat{\rho}_\mathrm{SD})$ is determined in the fit to data and used to model differences between data and simulation in $\varepsilon_\mathrm{QCD}(\hat{p}_\mathrm{T})$.

As a basis for the two-dimensional residual function, Bernstein polynomials are used. The i-th Bernstein basis polynomial of n-th degree with $i \in [0, \cdots, n]$ is defined for $x \in [0,1]$ as

$$b_i^n(x) = \binom{n}{i} x^i (1-x)^{n-i}. \tag{6.2}$$

The Bernstein basis is chosen over a standard polynomial because with the variable x bounded between 0 and 1 it is more stable numerically and the function is nonnegative [58]. The residual function is a linear combination of Bernstein polynomials

$$r(\hat{p}_\mathrm{T}, \hat{\rho}_\mathrm{SD}) = \sum_i^{n_{p_\mathrm{T}}} \sum_j^{n_{\rho_\mathrm{SD}}} a_{ij} b_j^{n_{p_\mathrm{T}}}(\hat{p}_\mathrm{T}) b_i^{n_{\rho_\mathrm{SD}}}(\hat{\rho}_\mathrm{SD}), \tag{6.3}$$

where n_{p_T} and n_{ρ_SD} are the orders of the Bernstein polynomials in $\hat{p}_\mathrm{T}$ and $\hat{\rho}_\mathrm{SD}$, respectively. The coefficients a_{ij} are free parameters in the fit to data.

An example of the residual function after a fit to data is shown in figure 4. To determine the optimal order of the Bernstein polynomials n_{ρ_SD} and n_{p_T}, the goodness of fit using the saturated model approach is evaluated for a series of orders. The resulting test statistics are then compared in F-tests and the orders of the polynomials are chosen to range from 1–2 for n_{p_T} and 2–6 for n_{ρ_SD} depending on the data-taking period.

7 Systematic uncertainties

The measurement of the differential $\mathrm{W}(\mathrm{q}\overline{\mathrm{q}}')$+jets cross section is subject to multiple sources of systematic uncertainties. These affect the m_SD in different ways, causing differences in shape, normalization, or both. Several such sources of systematic uncertainties are accounted for in the fit as nuisance parameters in the likelihood function.

Uncertainties related to the QCD background estimate are accounted for through the unconstrained parameters a_{ij} of the transfer function. Alternative functional forms for the transfer function (Chebyshev polynomials, exponentials of Bernstein polynomials) have been found to have a significantly smaller impact on the result than the accounted uncertainties on the parameters a_{ij} [58].

Uncertainties related to the jet energy scale calibration affect both the normalization through migrations of events between p_T bins, and the m_SD shape through variations in the subjet energy. The uncertainty in the measurement of the total luminosity of $138\,\mathrm{fb}^{-1}$ is estimated to be 1.6% [74–76]. This uncertainty is accounted for in the fits as normalization nuisance parameters for signal and background processes. The uncertainty in the trigger scale factors originates from the statistical uncertainties in the trigger efficiency measurement. Variations in the trigger scale factors are propagated to the p_T and m_SD and used as a shape uncertainty in the fit.

The number of interactions per bunch crossing is estimated from the measurements of the luminosity and the inclusive inelastic cross section of pp collisions. The simulation is reweighted to match the distribution of the number of interactions per bunch crossing in data.

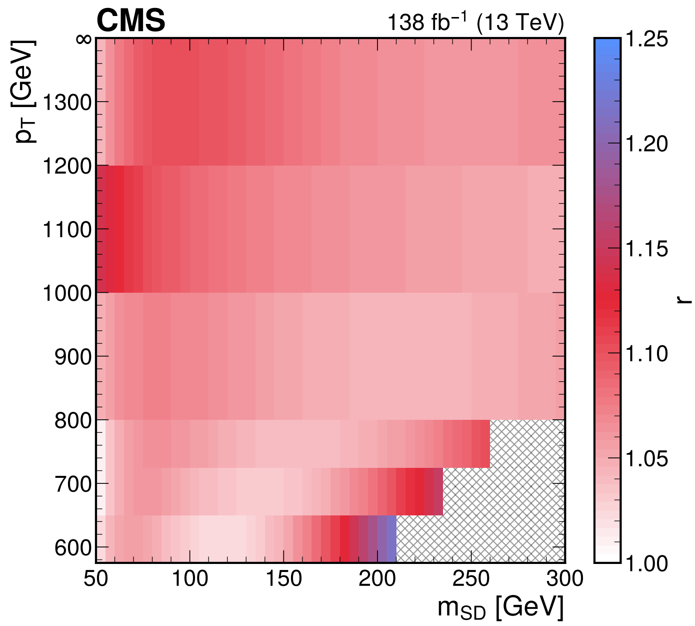

Figure 4. Residual function $r(\hat{p}_{\mathrm{T}}, \hat{\rho}_{\mathrm{SD}})$ obtained from a fit to data, when using the $P^{\mathrm{PN,DDT}}_{\mathrm{W vs.\ QCD}}$ as jet tagger. The arguments of the function r, $\hat{p}_{\mathrm{T}}$ and $\hat{\rho}_{\mathrm{SD}}$ are functions of m_{SD} and p_{T} and correspond to the normalized observables p_{T} and ρ_{SD}, scaled to lie in the interval $[0, 1]$. The hatched area is excluded from the analyses by selecting $\rho_{\mathrm{SD}} < -2.1$.

The inclusive inelastic cross section is varied up and down by 4.6% [77] and the reweighting is repeated. The uncertainty corresponds to the effect of these variations and is propagated to the p_{T} and m_{SD}. It is treated as a shape uncertainty for all simulated events.

Differences in jet tagging efficiencies between data and simulation in $\mathrm{W(q\overline{q}')}$+jets signal events are accounted for by an unconstrained nuisance parameter θ in the fit. This parameter allows for anticorrelated changes of the normalization in the pass and fail regions while conserving the total number of events,

$$\begin{aligned} N_{\mathrm{total}} &= N_{\mathrm{pass}} + N_{\mathrm{fail}} = \hat{N}_{\mathrm{pass}} + \hat{N}_{\mathrm{fail}} \\ &= \hat{\theta} N_{\mathrm{pass}} + \left[(1 - \hat{\theta}) \frac{N_{\mathrm{pass}}}{N_{\mathrm{fail}}} + 1 \right] N_{\mathrm{fail}}, \end{aligned} \tag{7.1}$$

where N_{total}, $\hat{N}_{\mathrm{pass}}$, and $\hat{N}_{\mathrm{fail}}$ are the total number of events and the best fit values of the number of events in the pass and fail regions, respectively. The parameter $\hat{\theta}$ denotes the best fit value of θ, while N_{pass} and N_{fail} are the initial number of events in the pass and fail regions, respectively.

The uncertainty in the modeling of initial-state radiation (ISR) and final-state radiation (FSR) is estimated by varying the respective parton shower renormalization scale up and down by a factor of two, and storing corresponding weights during the event generation. The effect is treated as a shape uncertainty for signal and background events by propagating the variations to the p_{T} and m_{SD} through a reweighting of simulated events. To account for uncertainties in the hadronization model of the $\mathrm{W(q\overline{q}')}$+jets signal process, we

JHEP07(2026)054

assign a shape uncertainty equal to the difference between the central simulation sample (MadGraph5_aMC@nlo+pythia) and an alternative generator (MadGraph5_aMC@nlo +herwig), which implements another hadronization model. This uncertainty mainly affects the tails of the W boson mass distribution, where nonperturbative effects dominate.

The higher-order QCD and EW correction systematic uncertainties for the $W(q\bar{q}')$+jets and $Z(q\bar{q})$+jets simulation is estimated from the envelope of the scale variations for the NLO QCD and NLO EW predictions derived in ref. [59]. The QCD and EW correction uncertainties are treated as separate shape uncertainties in the fit. Uncertainties related to parton distribution functions have been estimated to be a factor $\geq$3 smaller than those in the considered p_T range [59] and neglected.

To account for uncertainties in the prediction of the $t\bar{t}$ cross section and kinematics, a shape uncertainty is introduced. The up and down variations are constructed by comparing the p_T and m_{SD} distributions with and without applying the top quark p_T reweighting. In addition, normalization uncertainties are included as nuisance parameters with log-normal constraints amounting to 20% for $Z(q\bar{q})$+jets [78].

In figure 5, we summarize the effect of the systematic uncertainties in the reconstructed m_{SD}. The dominant shape effects can be attributed to uncertainties in the hadronization model, jet energy scale, and final-state shower. The jet energy scale and final-state shower mainly affect the region of the W boson mass peak ($70 < m_{SD}^{reco} < 110$ GeV). These lead to a shift of events from the peak region on top of a falling background, thus affecting most strongly the number of events at the right-hand side of the W boson mass peak ($90 < m_{SD}^{reco} < 110$ GeV). The size of the hadronization model uncertainty is smallest at the W boson mass peak and mainly affects the tails of the W boson mass distribution ($m_{SD}^{reco} < 70$ GeV and $m_{SD}^{reco} > 90$ GeV) where light-flavor quark and gluon jets dominate [22].

8 Unfolding

To obtain a measurement at the particle-level, detector effects are corrected for by unfolding the measured detector-level distribution. In the maximum-likelihood template fit with constraints for regularization, background subtraction and inversion of the detector response matrix R_{ij} are performed simultaneously in a global fit to the recorded collision data. This approach as detailed in the following is similar to the one outlined in ref. [79], though a maximum likelihood fit instead of a least-squares fit is used.

The signal strength modifiers μ_j are the ratios of the number of events predicted by the fit to data to the expected number of events at the particle level in simulation. The total number of expected events in bin i at the detector level is given by

$$y_i = \sum_{j=1}^{M} R_{ij}\mu_j x_j + b_i. \tag{8.1}$$

Here, the expectation value of the true number of events in bin j at the particle level is given by x_j and b_i denotes the total number of expected background events in bin i at the detector level. The response matrix R_{ij} is obtained from the simulation. It is constructed by filling events in bin i at the detector level, given that they were generated in bin j at the particle

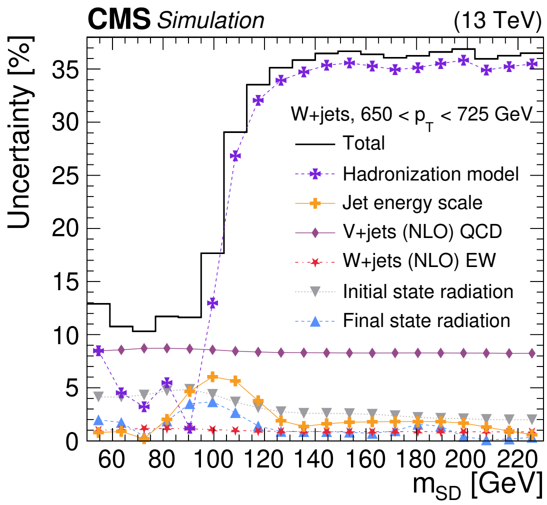

Figure 5. Summary of the effect of the systematic uncertainties in the reconstructed SD jet mass in the $W(q\overline{q}')$+jets signal sample in a representative p_T bin. The dominant shape effects can be attributed to uncertainties in the hadronization model, jet energy scale, and final-state shower. The jet energy scale and final state shower mainly affect the region of the W boson mass peak ($70 < m_{SD} < 110\,GeV$).

level. Events are only considered in the response matrix if the selected jets at the detector and particle level can be matched to the generated W boson. Acceptance and efficiency effects originating from events falling out of the fiducial phase space by failing either the detector- or particle-level selections, or the matching criterion, are not included in the response matrix. Instead, these are accounted for in a factorized approach. Events that pass the detector-level selection, but do not have a matching jet at the particle level or are not matched to a generated W boson are treated as background in the fit. Events that fail the detector-level selection or the matching criterion but pass the particle-level selection are accounted for with an acceptance correction. The resulting response matrix is shown in figure 6.

The best fit values of the parameters of interest $\vec{\mu}$ are obtained by minimizing the negative log-likelihood function

$$-2\ln\mathcal{L}(\vec{\mu}) = -2\sum_{i}^{N}\ln P(n_i, y_i), \tag{8.2}$$

where n_i is the total number of events in data in bin i at the detector level and $P(n_i, y_i)$ refers to the Poisson distribution.

We include all bins in m_{SD} and p_T in the fit, where each bin is split into pass and fail regions from the jet substructure tagger requirements. The fit is performed in all four eras of data-taking simultaneously by using the product of the individual likelihoods with one common set of parameters of interest. We measure one signal strength modifier μ_j per particle-level bin j, which scales the prediction in each particle-level bin to obtain the measured cross sections.

The regularization of the multidimensional distribution is performed using Tikhonov regularization [80], adding a penalty term with a strength parameter τ to the negative log-

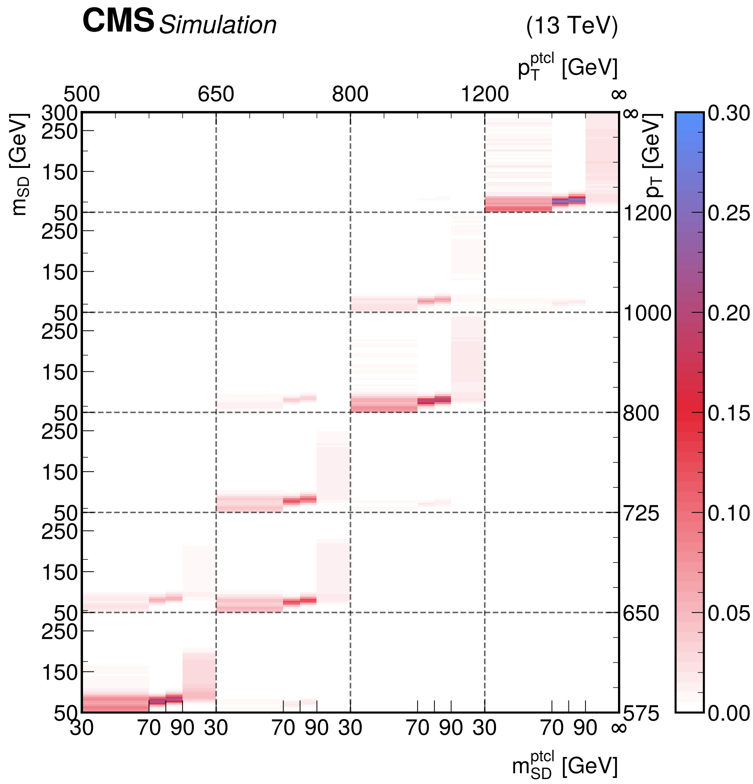

Figure 6. Response matrix obtained for selected events in simulation. The matrix is obtained from a sum of all data-taking eras. The grey dashed lines separate the individual p_T bins. The binning within each p_T bin corresponds to the m_{SD} binning.

likelihood function. We choose a regularization strength parameter $\tau = 0.59$ by minimizing an average global correlation coefficient which was found to vary only mildly (by 0.5%) over a wide range ($0.1 < \tau < 2$) of the regularization strength parameter. Regularization is necessary to obtain accurate measurements in the lowest and highest particle-level m_{SD} bins, where acceptance is low and backgrounds are more dominant.

To estimate the bias and over- or under-coverage introduced by the regularization, a series of tests is performed using pseudo-data in the fit instead of collision data. Replacing data with signal simulation yields perfect closure with the expectation. To test the model against statistical fluctuations in the pseudo-data, the pseudo-data are perturbed by generating 500 toy data sets. We then compute the pull distribution of the maximum likelihood estimators $\hat{\mu}_j$ of the signal strength modifiers. The mean of the distribution of pulls is consistent with zero within one standard deviation. To further test for biases introduced by the regularization, the same tests are performed using statistically independent pseudo-data, yielding the same conclusions.

To better understand the dominant sources of uncertainty in representative p_T^{ptcl} and m_{SD}^{ptcl} bins, the impacts of key groups of systematic uncertainties in the signal strength modifiers μ_j are summarized in table 3 for the $P_{\text{Wvs. QCD}}^{\text{PN,DDT}}$ tagger. The largest contributions to the total uncertainty near the m_W peak (second column) are the W tagging efficiency, the V+jets QCD NLO corrections, the Z+jets normalization, FSR and hadronization model, reaching

Uncertainty	Impact in $m_{\mathrm{SD}}^{\mathrm{ptcl}}$ bin	
	$80 < m_{\mathrm{SD}}^{\mathrm{ptcl}} < 90\,\mathrm{GeV}$	$m_{\mathrm{SD}}^{\mathrm{ptcl}} > 90\,\mathrm{GeV}$
Jet energy scale	4.8 %	23.9 %
W tagging efficiency	11.9 %	14.3 %
Pileup reweighting	1.1 %	3.1 %
Trigger scale factor	0.7 %	1.1 %
Integrated luminosity	1.6 %	1.3 %
QCD multijet estimate	3.6 %	13.9 %
Z+jets normalization	6.6 %	3.0 %
Top quark p_{T} reweight	0.3 %	0.9 %
V+jets QCD NLO	14.4 %	17.7 %
W+jets EW NLO	1.3 %	0.7 %
Z+jets EW NLO	<0.1 %	0.2 %
FSR	12.2 %	17.4 %
ISR	3.7 %	4.9 %
Hadronization model	12.4 %	15.5 %

Table 3. Summary of systematic uncertainties and their impact on the measurement in the $650 < p_{\mathrm{T}}^{\mathrm{ptcl}} < 800\,\mathrm{GeV}$ bin and two representative $m_{\mathrm{SD}}^{\mathrm{ptcl}}$ bins, using the $P_{\mathrm{Wvs.\ QCD}}^{\mathrm{PN,DDT}}$ tagger.

up to 14.4%. Outside the m_{W} peak region (third column), the jet energy scale and the QCD multijet estimate also contribute up to 23.9%.

9 Results

The measurement of the fiducial cross section is double differential in $m_{\mathrm{SD}}^{\mathrm{ptcl}}$ and $p_{\mathrm{T}}^{\mathrm{ptcl}}$ and uses the $P_{\mathrm{Wvs.\ QCD}}^{\mathrm{PN,DDT}}$ approach. Tabulated results are provided in the HEPData record for this analysis [81]. The correlation matrix in figure 7 shows the correlation coefficients of the individual particle-level bins. The $m_{\mathrm{SD}}^{\mathrm{ptcl}}$ bins in the different $p_{\mathrm{T}}^{\mathrm{ptcl}}$ bins are shown unrolled, where the grey dashed lines indicate the $p_{\mathrm{T}}^{\mathrm{ptcl}}$ bins boundaries. The highest correlations are found to be among neighboring bins, both along the $m_{\mathrm{SD}}^{\mathrm{ptcl}}$ and $p_{\mathrm{T}}^{\mathrm{ptcl}}$ axes. The latter ones are similar for all $m_{\mathrm{SD}}^{\mathrm{ptcl}}$ bins, but smaller on average than the correlations between neighboring bins along the $m_{\mathrm{SD}}^{\mathrm{ptcl}}$ axis. The highest anticorrelations are found between the first two and last two $m_{\mathrm{SD}}^{\mathrm{ptcl}}$ bins in the third and fourth $p_{\mathrm{T}}^{\mathrm{ptcl}}$ bins.

The extracted jet mass distributions are shown in figure 8. For the purpose of display the differential fiducial cross section $\mathrm{d}\sigma/\mathrm{d}m_{\mathrm{SD}}$ is shown in bins of $p_{\mathrm{T}}^{\mathrm{ptcl}}$. The unfolded data are shown as black markers with the total uncertainty (the square roots of the diagonal elements of the covariance matrix containing statistical $\oplus$ systematic uncertainty) drawn as black bars. The V+jets theory prediction from MadGraph5_aMC@NLO+PYTHIA has

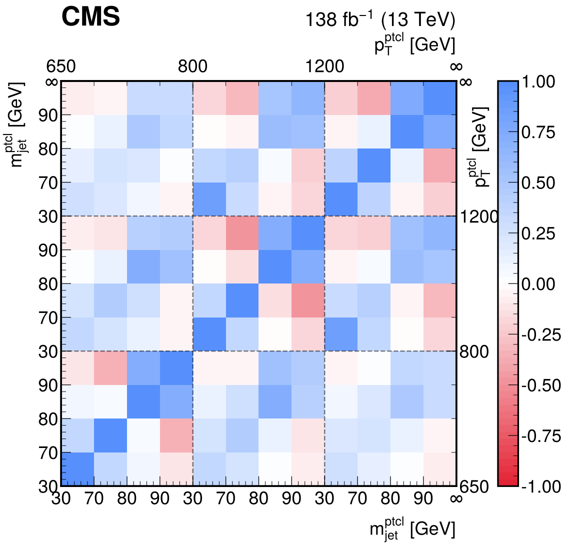

Figure 7. Correlation matrix of the maximum likelihood estimators of the signal strength modifiers $\hat{\mu}_{p_{\mathrm{T}},\, m_{\mathrm{SD}}}$ with inclusion of an $N_2^{(1)} < 0.2$ selection in the particle-level definition. The plot shows the matrix from the fit to the data using $P^{\mathrm{PN,DDT}}_{\mathrm{Wvs.\ QCD}}$. The grey dashed lines indicate the individual $p_{\mathrm{T}}^{\mathrm{ptcl}}$ bins. The binning within each $p_{\mathrm{T}}^{\mathrm{ptcl}}$ vs. $p_{\mathrm{T}}^{\mathrm{ptcl}}$ bin corresponds to the $m_{\mathrm{SD}}^{\mathrm{ptcl}}$ vs. $m_{\mathrm{SD}}^{\mathrm{ptcl}}$ binning.

LO+MLM accuracy with NLO (QCD and EW) corrections and is depicted as a blue curve. The corresponding theory uncertainty is the sum in quadrature of parton shower variations and hadronization model uncertainty, as well as the two envelopes of systematic uncertainties characterizing missing higher-order QCD and EW corrections [59], as detailed in the previous section, and is drawn as a light shaded blue band. The purely perturbative uncertainties are also overlaid as a dark, shaded blue band.

We quantify the agreement of the data with the prediction using a goodness-of-fit test based on the saturated model [82] and observe p-values larger than 0.13 for all four data-taking periods. The unfolded data distributions agree with the predictions within the total uncertainty in all $p_{\mathrm{T}}^{\mathrm{ptcl}}$ bins. The data in the first $p_{\mathrm{T}}^{\mathrm{ptcl}}$ bin are generally in better agreement with the simulation concerning both the normalization as well as the shape of the distributions. In the last two $p_{\mathrm{T}}^{\mathrm{ptcl}}$ bins, we observe a shift in the peak position in the unfolded data compared to the simulation, that is, however, covered by the uncertainties and their correlations.

The upper and lower ends of the $m_{\mathrm{SD}}^{\mathrm{ptcl}}$ spectrum contain events where not the W boson jet, but the recoiling quark/gluon jet is measured. Thus, in the first $m_{\mathrm{SD}}^{\mathrm{ptcl}}$ bin, the predicted yield depends on the modeling of nonperturbative effects, which is model dependent. Figure 9 shows the distributions without and with the $N_2^{(1)} < 0.2$ selection at the particle level, where the individual distributions in each $p_{\mathrm{T}}^{\mathrm{ptcl}}$ bin for $p_{\mathrm{T}}^{\mathrm{ptcl}} > 650\,\mathrm{GeV}$ have been added. The predictions without the $N_2^{(1)} < 0.2$ selection give a larger fraction of events in the lowest and highest m_{SD} bins, where the signal is contaminated by light-flavor quark and gluon jets.

The measured jet mass distribution is sensitive to the W boson mass. In the following, we quantify the sensitivity of the m_{SD} distribution to the W boson mass and quote a first measurement of the W boson mass in an all-jets final state at a hadron collider. We compare multiple LO predictions (called templates in the following) generated with PYTHIA with

JHEP07(2026)054

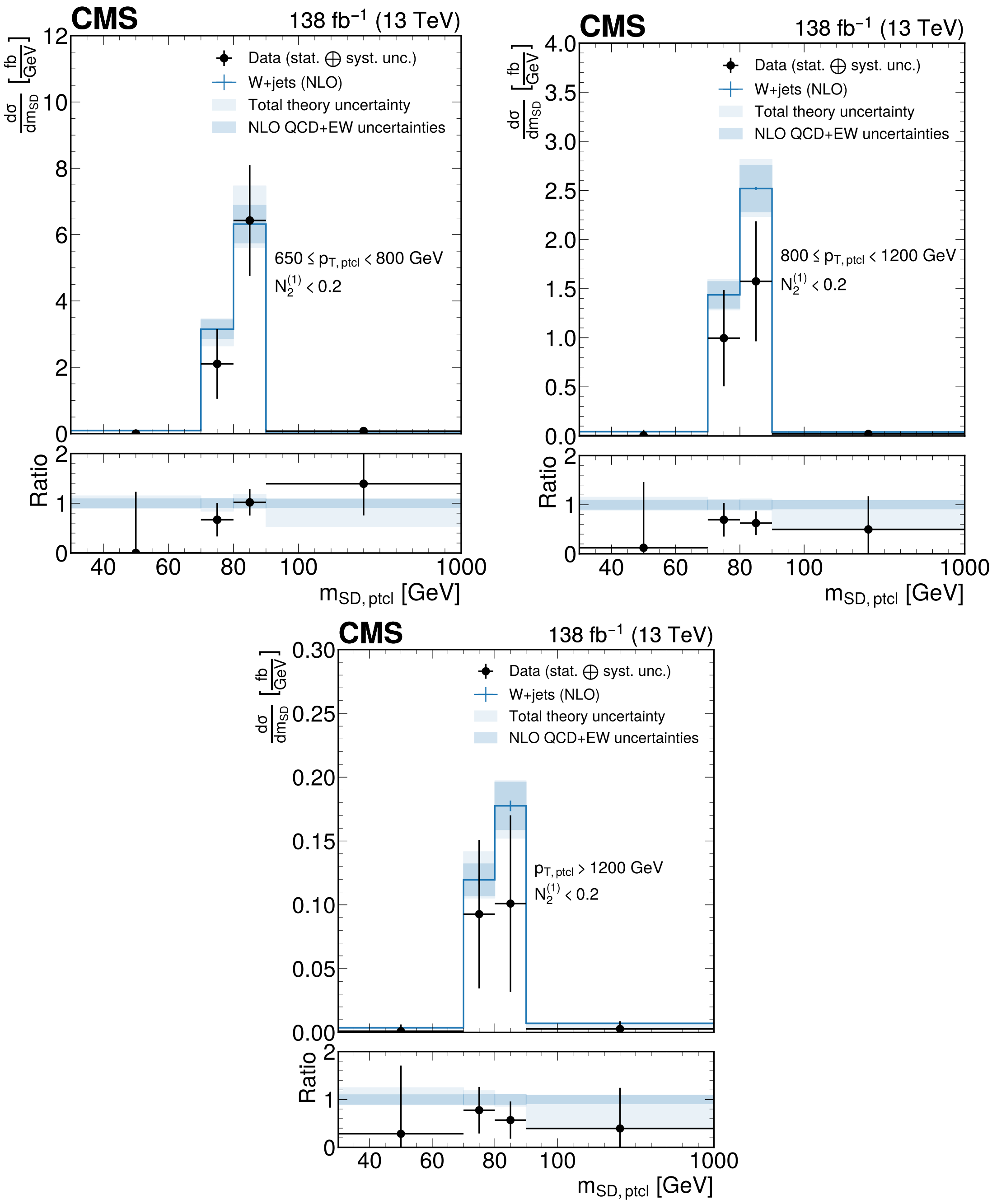

Figure 8. Unfolded and background subtracted jet mass distribution at the particle level for each p_T^{ptcl} bin obtained with $P^{PN,DDT}_{Wvs.\ QCD}$. The fiducial measurement region at the particle level includes the $N_2^{(1)} < 0.2$ selection. The unfolded data are shown as black markers with the total uncertainty indicated as error bar. The blue lines show the predictions from MadGraph5_aMC@NLO+pythia at LO with MLM matching and supplemented by NLO QCD and EW corrections with the statistical uncertainty indicated as error bar. The theory uncertainty is the sum in quadrature of parton shower variations and the hadronization model uncertainty, as well as the uncertainties in the QCD and EW corrections, and is drawn as a light shaded blue band. The purely perturbative uncertainties are overlaid as a dark, shaded blue band.

JHEP07(2026)054

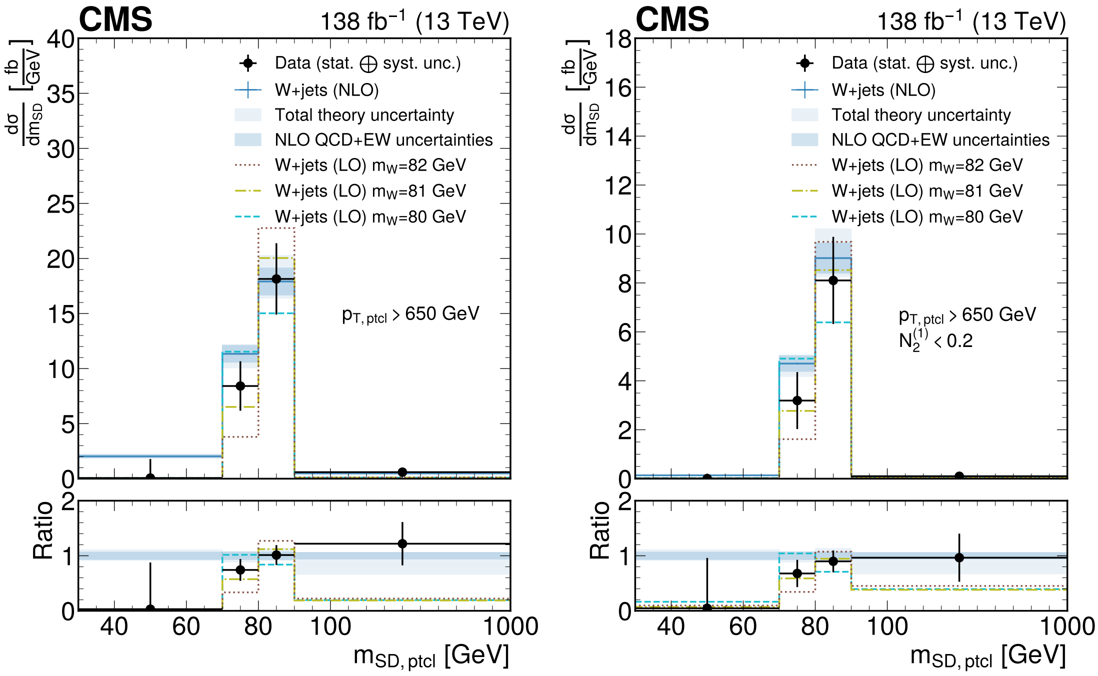

Figure 9. Unfolded and background subtracted jet mass distribution at the particle level for $p_T^{ptcl} >$ 650 GeV, obtained by summing all p_T^{ptcl} bins. The results are obtained using the $P^{PN,DDT}_{Wvs.\ QCD}$ tagger without (left) and with (right) the $N_2^{(1)} < 0.2$ selection at the particle level. The unfolded data are shown as black markers. The blue lines show the predictions from MadGraph5_aMC@NLO+pythia at LO with MLM matching and supplemented by NLO QCD and EW corrections. The theory uncertainty is the sum in quadrature of parton shower variations and the hadronization model uncertainty, as well as the uncertainties in the QCD and EW corrections, and is drawn as a light shaded blue band. The purely perturbative uncertainties are overlaid as a dark, shaded blue band. Predictions with different values of the W boson mass generated with pythia at LO and scaled to match the total number of events in data are overlaid.

JHEP07(2026)054

different values of generated W boson mass: 79.0, 80.0, 80.385 (pythia default), 81.0, 82.0 GeV to the unfolded data distributions. Higher-order corrections to the theory prediction are not accounted for in this estimate, as the statistical uncertainty dominates over the theoretical uncertainties. In order to minimize the impact of shower and hadronization effects on the result, we use cross sections obtained for $N_2^{(1)} < 0.2$ at the particle level. We only use the two bins in m_{SD} that fall into the W boson mass peak with $70 < m_{SD} < 90$ GeV, integrating over $p_T^{ptcl} > 650$ GeV, and use the normalized cross section, where the normalization is done for the peak region only. We carry out a fit using the linear template fit package [83] to estimate the W boson mass parameter. We account for the same sources of uncertainties as in the differential cross section measurement.

A closure test is carried out by replacing the data with the pythia simulation with a certain W boson mass parameter, and then measuring m_W using the remaining pythia templates. We find a linear dependence between the input and measured mass consistent with unity slope. We also check the consistency of the method by measuring the mass of the MadGraph5_aMC@NLO+pythia and MadGraph5_aMC@NLO+herwig samples

Uncertainty	Impact on m_{W} [GeV]
Statistical	0.31
QCD multijet estimate	0.18
Stat. + bkg	0.36
Jet energy scale	0.36
W tagging efficiency	0.07
Pileup reweighting	0.04
Trigger scale factor	0.02
Integrated luminosity	0.02
Z+jets normalization	0.17
Top quark p_{T} reweight	0.04
V+jets QCD NLO	0.03
W+jets EW NLO	0.02
Z+jets EW NLO	0.01
FSR	0.01
ISR	0.02
Hadronization model	0.02
Other syst.	0.41
Total	0.55

Table 4. Summary of systematic uncertainties and their impact on the m_{W} measurement.

JHEP07(2026)054

with a generated W boson mass of 80.419 GeV using templates from PYTHIA, resulting in 80.30 ± 0.33 GeV and 80.54 ± 0.37 GeV, respectively, where the uncertainty is the total uncertainty, including the statistical and systematic components.

The result of the template fit to data is 80.81 ± 0.55 (total) GeV, or when separating statistical and background uncertainty sources, 80.81 ± 0.36 (stat. + bkg) $\pm\, 0.41$ (other syst.) GeV. The impact of individual uncertainties on the m_{W} measurement is given in table 4. Uncertainties affecting the position and shape of the m_{W} peak, such as the statistical uncertainty, the background uncertainty and the jet energy scale are most relevant uncertainties for the m_{W} parameter estimation. For consistency with other measurements of the W boson mass, we translate these results to the frequently used mass parameter in a Breit-Wigner distribution with mass-dependent width by adding 27 MeV [84], resulting in 80.83 ± 0.55 GeV. The result is consistent with previous m_{W} measurements making use of leptonic final states, though not yet competitive. It represents a first step towards a potentially competitive measurement at the HL-LHC [15].

10 Summary

The jet mass of W bosons decaying to a quark-antiquark pair is measured in W+jets events from proton-proton collisions at the LHC at a center-of-mass energy $\sqrt{s} = 13\,\text{TeV}$. The data were collected by the CMS experiment in 2016–2018 and correspond to an integrated luminosity of $138\,\text{fb}^{-1}$. The measurement considers W bosons with large momenta, resulting in strongly collimated decay products that are reconstructed in a single large-radius jet. Jets initiated by W bosons with a characteristic two-prong substructure are distinguished from single light-flavor quark and gluon-initiated background jets using a selection based on the substructure of these jets. The jet mass is measured using the soft-drop (SD) algorithm, which suppresses soft and wide-angle radiation that can obscure the resonance peak of the W boson at its rest mass. We report the first measurement of the double-differential cross section in bins of the jet transverse momentum and SD mass. The unfolded data are found to be in agreement with predictions from simulations at leading order with additional partons added to the matrix element computation, supplemented by next-to-leading order quantum chromodynamics and electroweak corrections. A W boson mass of $80.83 \pm 0.55\,\text{GeV}$ in a scheme with mass-dependent width is obtained, achieving the smallest uncertainty available today from an all-jets final state at a hadron collider.

Acknowledgments

We congratulate our colleagues in the CERN accelerator departments for the excellent performance of the LHC and thank the technical and administrative staffs at CERN and at other CMS institutes for their contributions to the success of the CMS effort. In addition, we gratefully acknowledge the computing centers and personnel of the Worldwide LHC Computing Grid and other centers for delivering so effectively the computing infrastructure essential to our analyses. Finally, we acknowledge the enduring support for the construction and operation of the LHC, the CMS detector, and the supporting computing infrastructure provided by the following funding agencies: SC (Armenia), BMBWF and FWF (Austria); FNRS and FWO (Belgium); CNPq, CAPES, FAPERJ, FAPERGS, and FAPESP (Brazil); MES and BNSF (Bulgaria); CERN; CAS, MoST, and NSFC (China); MINCIENCIAS (Colombia); MSES and CSF (Croatia); RIF (Cyprus); SENESCYT (Ecuador); ERC PRG and PSG, TARISTU24-TK10 and MoER TK202 (Estonia); Academy of Finland, MEC, and HIP (Finland); CEA and CNRS/IN2P3 (France); SRNSF (Georgia); BMFTR, DFG, and HGF (Germany); GSRI (Greece); NKFIH (Hungary); DAE and DST (India); IPM (Iran); SFI (Ireland); INFN (Italy); MSIT and NRF (Republic of Korea); MES (Latvia); LMTLT (Lithuania); MOE and UM (Malaysia); BUAP, CINVESTAV, CONACYT, LNS, SEP, and UASLP-FAI (Mexico); MOS (Montenegro); MBIE (New Zealand); PAEC (Pakistan); MES, NSC, and NAWA (Poland); FCT (Portugal); MESTD (Serbia); MICIU/AEI and PCTI (Spain); MOSTR (Sri Lanka); Swiss Funding Agencies (Switzerland); MST (Taipei); MHESI (Thailand); TUBITAK and TENMAK (Türkiye); NASU (Ukraine); STFC (United Kingdom); DOE and NSF (U.S.A.).

Individuals have received support from the Marie-Curie program and the European Research Council and Horizon 2020 Grant, contract Nos. 675440, 724704, 752730, 758316, 765710, 824093, 101115353, 101002207, 101001205, and COST Action CA16108 (European Union); the Leventis Foundation; the Alfred P. Sloan Foundation; the Alexander von Humboldt Foundation; the Science Committee, project no. 22rl-037 (Armenia); the Fonds pour la Formation à la Recherche dans l'Industrie et dans l'Agriculture (FRIA) and Fonds voor Wetenschappelijk Onderzoek contract No. 1228724N (Belgium); the Beijing Municipal Science & Technology Commission, No. Z191100007219010, the Fundamental Research Funds for the Central Universities, the Ministry of Science and Technology of China under Grant No. 2023YFA1605804, the Natural Science Foundation of China under Grant No. 12535004, and USTC Research Funds of the Double First-Class Initiative No. YD2030002017 (China); the Ministry of Education, Youth and Sports (MEYS) of the Czech Republic; the Shota Rustaveli National Science Foundation, grant FR-22-985 (Georgia); the Deutsche Forschungsgemeinschaft (DFG), among others, under Germany's Excellence Strategy — EXC 2121 "Quantum Universe" — 390833306, and under project number 400140256 — GRK2497; the Hellenic Foundation for Research and Innovation (HFRI), Project Number 2288 (Greece); the Hungarian Academy of Sciences, the New National Excellence Program — ÚNKP, the NKFIH research grants K 131991, K 133046, K 138136, K 143460, K 143477, K 146913, K 146914, K 147048, 2020-2.2.1-ED-2021-00181, TKP2021-NKTA-64, and 2025-1.1.5-NEMZ_KI-2025-00004 (Hungary); the Council of Science and Industrial Research, India; ICSC — National Research Center for High Performance Computing, Big Data and Quantum Computing, FAIR — Future Artificial Intelligence Research, and CUP I53D23001070006 (Mission 4 Component 1), funded by the NextGenerationEU program, the Italian Ministry of University and Research (MUR) under Bando PRIN 2022 — CUP I53C24002390006, PRIN PRIMULA 2022RBYK7T (Italy); the Latvian Council of Science; the Ministry of Education and Science, project no. 2022/WK/14, and the National Science Center, contracts Opus 2021/41/B/ST2/01369, 2021/43/B/ST2/01552, 2023/49/B/ST2/03273, and the NAWA contract BPN/PPO/2021/1/00011 (Poland); the Fundação para a Ciência e a Tecnologia (Portugal); the National Priorities Research Program by Qatar National Research Fund; MICIU/AEI/10.13039/501100011033, ERDF/EU, "European Union NextGenerationEU/PRTR", projects PID2022-142604OB-C21, PID2022-139519OB-C21, PID2023-147706NB-I00, PID2023-148896NB-I00, PID2023-146983NB-I00, PID2023-147115NB-I00, PID2023-148418NB-C41, PID2023-148418NB-C42, PID2023-148418NB-C43, PID2023-148418NB-C44, PID2024-158190NB-C22, RYC2021-033305-I, RYC2024-048719-I, CNS2023-144781, CNS2024-154769 and Plan de Ciencia, Tecnología e Innovación de Asturias, Spain; the Chulalongkorn Academic into Its 2nd Century Project Advancement Project, the National Science, Research and Innovation Fund program IND_FF_68_369_2300_097, and the Program Management Unit for Human Resources & Institutional Development, Research and Innovation, grant B39G680009 (Thailand); the Eric & Wendy Schmidt Fund for Strategic Innovation through the CERN Next Generation Triggers project under grant agreement number SIF-2023-004; the Kavli Foundation; the Nvidia Corporation; the SuperMicro Corporation; the Welch Foundation, contract C-1845; and the Weston Havens Foundation (U.S.A.).

JHEP07(2026)054

A Full set of reconstructed m_{SD} distributions

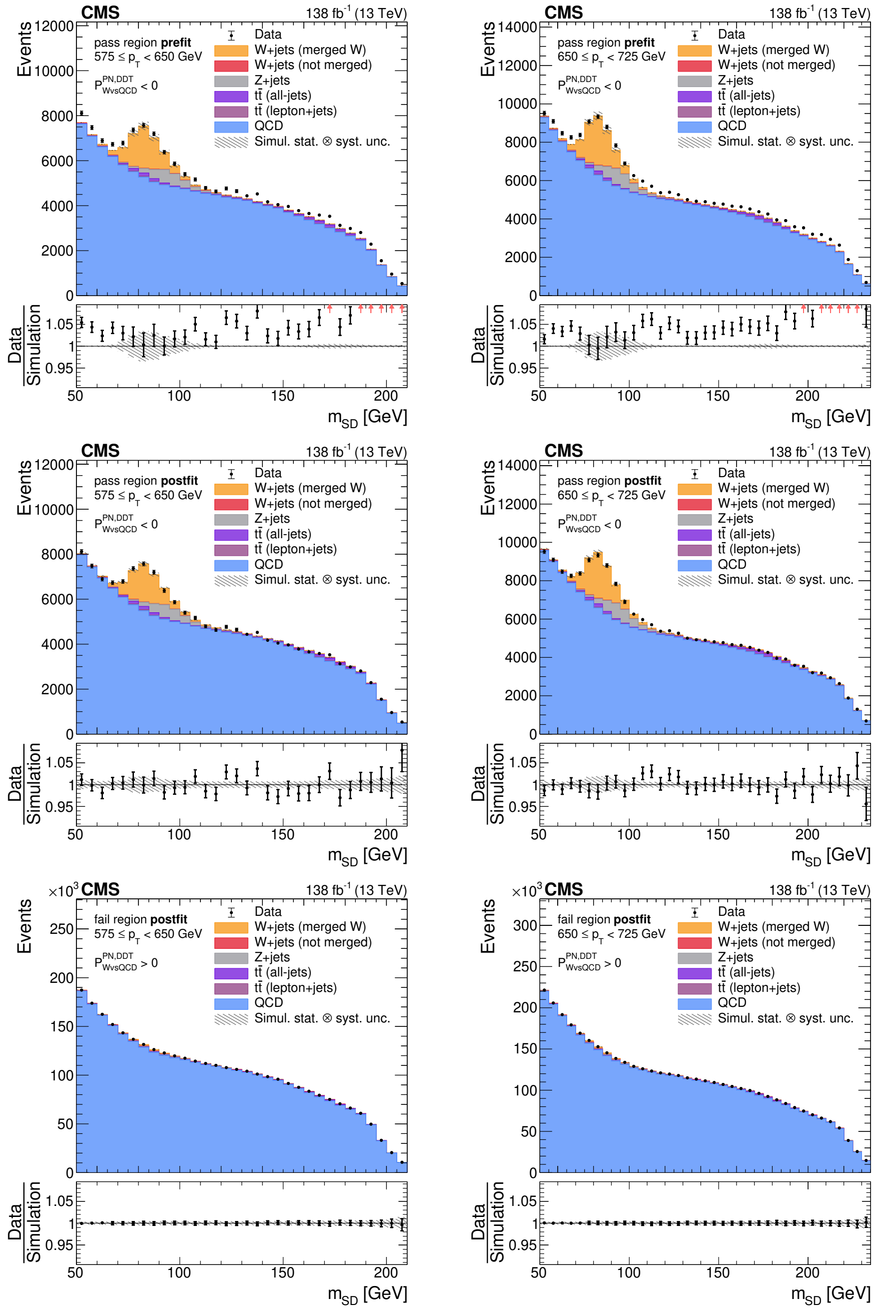

Figure 10. Reconstructed m_{SD} distributions in the p_{T} bin with $575 < p_{\mathrm{T}} < 650\,\mathrm{GeV}$ (left) and $650 < p_{\mathrm{T}} < 725\,\mathrm{GeV}$ (right) in the control region (lower row) and signal region before (upper row) and after (middle row) the background estimation and a fit to the data. All four data-taking periods are combined, resulting in a total integrated luminosity of $138\,\mathrm{fb}^{-1}$. The lower panels show the data-to-simulation ratio. The error bars correspond to the statistical uncertainty in the data. In the upper row, the dashed band corresponds to the total uncertainty excluding the uncertainty on the QCD background estimate, while in the middle and lower row it corresponds to the total uncertainty on the background after a fit to the data distribution.

JHEP07(2026)054

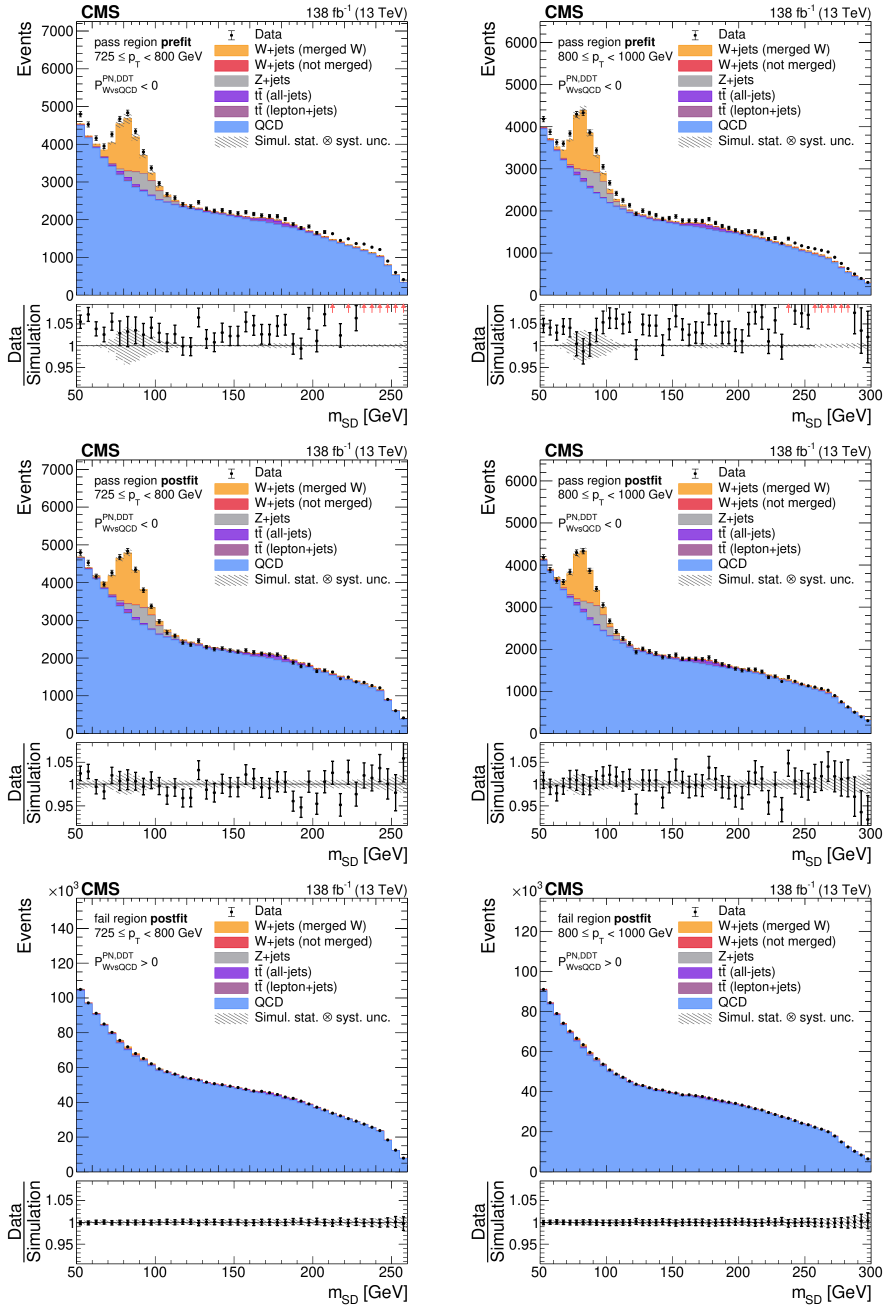

Figure 11. Reconstructed m_{SD} distributions in the p_{T} bin with $725 < p_{\mathrm{T}} < 800\,\mathrm{GeV}$ (left) and $800 < p_{\mathrm{T}} < 100\,\mathrm{GeV}$ (right) in the control region (lower row) and signal region before (upper row) and after (middle row) the background estimation and a fit to the data. All four data-taking periods are combined, resulting in a total integrated luminosity of $138\,\mathrm{fb}^{-1}$. The lower panels show the data-to-simulation ratio. The error bars correspond to the statistical uncertainty in the data. In the upper row, the dashed band corresponds to the total uncertainty excluding the uncertainty on the QCD background estimate, while in the middle and lower row it corresponds to the total uncertainty on the background after a fit to the data distribution.

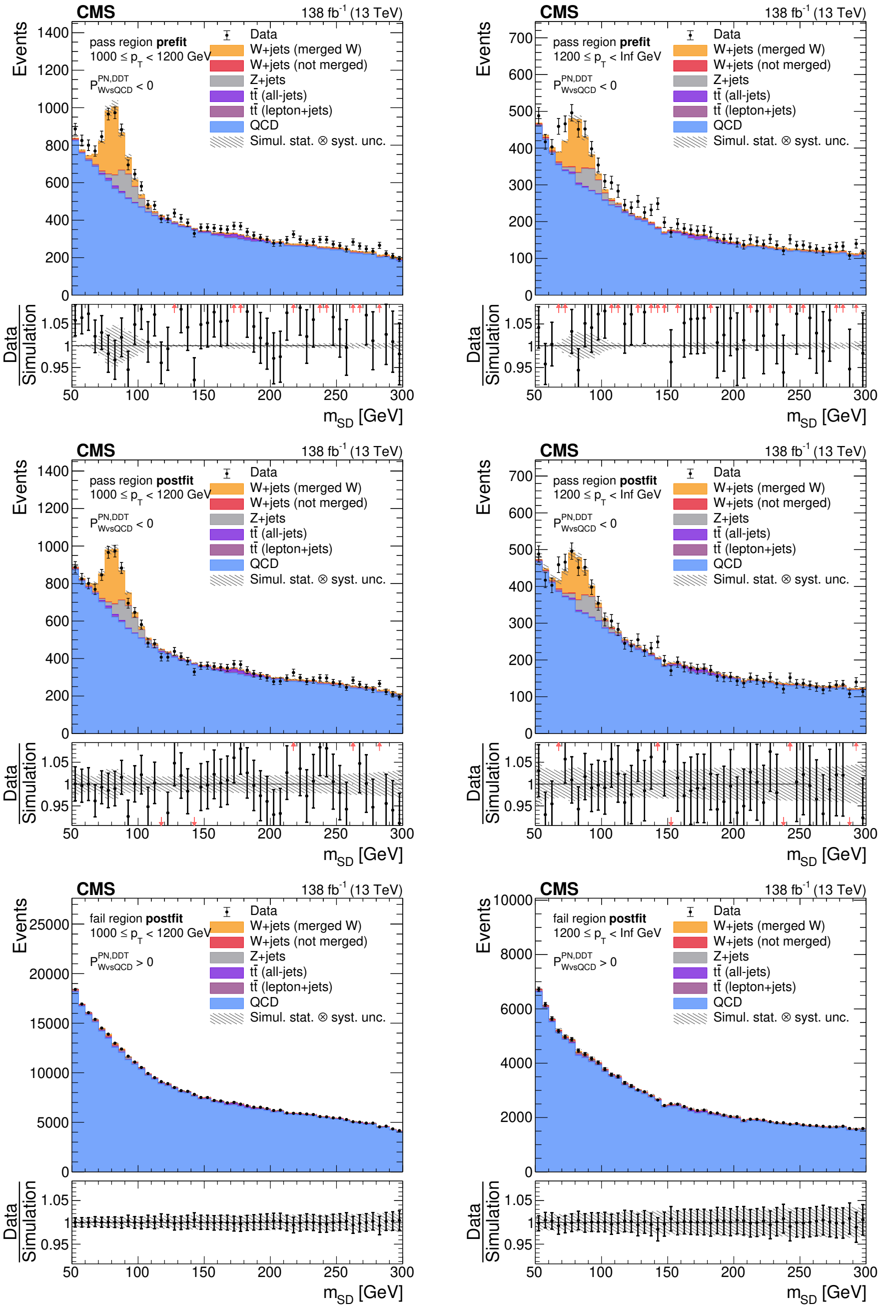

Figure 12. Reconstructed m_{SD} distributions in the p_{T} bin with $1000 < p_{\mathrm{T}} < 1200\,\mathrm{GeV}$ (left) and $p_{\mathrm{T}} > 1200\,\mathrm{GeV}$ (right) in the control region (lower row) and signal region before (upper row) and after (middle row) the background estimation and a fit to the data. All four data-taking periods are combined, resulting in a total integrated luminosity of $138\,\mathrm{fb}^{-1}$. The lower panels show the data-to-simulation ratio. The error bars correspond to the statistical uncertainty in the data. In the upper row, the dashed band corresponds to the total uncertainty excluding the uncertainty on the QCD background estimate, while in the middle and lower row it corresponds to the total uncertainty on the background after a fit to the data distribution.

Data Availability Statement. Release and preservation of data used by the CMS Collaboration as the basis for publications is guided by the CMS data preservation, re-use and open access policy.

Code Availability Statement. The CMS core software is publicly available on GitHub.

References

[1] ALEPH et al. collaborations, *Electroweak measurements in electron-positron collisions at W-boson-pair energies at LEP*, *Phys. Rept.* **532** (2013) 119 [arXiv:1302.3415] [INSPIRE].

[2] D0 collaboration, *Measurement of the W boson mass with the D0 detector*, *Phys. Rev. Lett.* **108** (2012) 151804 [arXiv:1203.0293] [INSPIRE].

[3] CDF collaboration, *High-precision measurement of the W boson mass with the CDF II detector*, *Science* **376** (2022) 170 [INSPIRE].

[4] ATLAS collaboration, *Measurement of the W-boson mass in pp collisions at $\sqrt{s} = 7$ TeV with the ATLAS detector*, *Eur. Phys. J. C* **78** (2018) 110 [*Erratum ibid.* **78** (2018) 898] [arXiv:1701.07240] [INSPIRE].

[5] LHCb collaboration, *Measurement of the W boson mass*, *JHEP* **01** (2022) 036 [arXiv:2109.01113] [INSPIRE].

[6] ATLAS collaboration, *Measurement of the W-boson mass and width with the ATLAS detector using proton–proton collisions at $\sqrt{s} = 7$ TeV*, *Eur. Phys. J. C* **84** (2024) 1309 [arXiv:2403.15085] [INSPIRE].

[7] CMS collaboration, *High-precision measurement of the W boson mass with the CMS experiment*, *Nature* **652** (2026) 321 [arXiv:2412.13872] [INSPIRE].

[8] Particle Data Group collaboration, *Review of particle physics*, *Phys. Rev. D* **110** (2024) 030001 [INSPIRE].

[9] S. Marzani, G. Soyez and M. Spannowsky, *Looking inside jets: an introduction to jet substructure and boosted-object phenomenology*, Springer (2019) [DOI:10.1007/978-3-030-15709-8] [INSPIRE].

[10] A.J. Larkoski, I. Moult and B. Nachman, *Jet substructure at the Large Hadron Collider: a review of recent advances in theory and machine learning*, *Phys. Rept.* **841** (2020) 1 [arXiv:1709.04464] [INSPIRE].

[11] R. Kogler et al., *Jet substructure at the Large Hadron Collider: experimental review*, *Rev. Mod. Phys.* **91** (2019) 045003 [arXiv:1803.06991] [INSPIRE].

[12] R. Kogler, *Advances in jet substructure at the LHC: algorithms, measurements and searches for new physical phenomena*, Springer (2021) [DOI:10.1007/978-3-030-72858-8] [INSPIRE].

[13] UA2 collaboration, *Search for decays of the $W^{\pm}$ and Z bosons into quark-anti-quark pairs*, *Phys. Lett. B* **186** (1987) 452 [INSPIRE].

[14] CDF collaboration, *Observation of hadronic W decays in $t\bar{t}$ events with the collider detector at Fermilab*, *Phys. Rev. Lett.* **80** (1998) 5720 [hep-ex/9711004] [INSPIRE].

JHEP07(2026)054

[15] M. Freytsis et al., *Prospects for a measurement of the W boson mass in the all-jets final state at hadron colliders*, *JHEP* **02** (2019) 003 [arXiv:1807.07454] [INSPIRE].

[16] M. Dasgupta, A. Fregoso, S. Marzani and G.P. Salam, *Towards an understanding of jet substructure*, *JHEP* **09** (2013) 029 [arXiv:1307.0007] [INSPIRE].

[17] J.M. Butterworth, A.R. Davison, M. Rubin and G.P. Salam, *Jet substructure as a new Higgs search channel at the LHC*, *Phys. Rev. Lett.* **100** (2008) 242001 [arXiv:0802.2470] [INSPIRE].

[18] A.J. Larkoski, S. Marzani, G. Soyez and J. Thaler, *Soft drop*, *JHEP* **05** (2014) 146 [arXiv:1402.2657] [INSPIRE].

[19] CMS collaboration, *The CMS experiment at the CERN LHC*, 2008 *JINST* **3** S08004 [INSPIRE].

[20] ATLAS collaboration, *Jet mass and substructure of inclusive jets in $\sqrt{s} = 7$ TeV pp collisions with the ATLAS experiment*, *JHEP* **05** (2012) 128 [arXiv:1203.4606] [INSPIRE].

[21] ATLAS collaboration, *Measurement of the soft-drop jet mass in pp collisions at $\sqrt{s} = 13$ TeV with the ATLAS detector*, *Phys. Rev. Lett.* **121** (2018) 092001 [arXiv:1711.08341] [INSPIRE].

[22] CMS collaboration, *Measurements of the differential jet cross section as a function of the jet mass in dijet events from proton-proton collisions at $\sqrt{s} = 13$ TeV*, *JHEP* **11** (2018) 113 [arXiv:1807.05974] [INSPIRE].

[23] CMS collaboration, *Measurement of the jet mass in highly boosted $t\bar{t}$ events from pp collisions at $\sqrt{s} = 8$ TeV*, *Eur. Phys. J. C* **77** (2017) 467 [arXiv:1703.06330] [INSPIRE].

[24] CMS collaboration, *Measurement of the jet mass distribution and top quark mass in hadronic decays of boosted top quarks in pp collisions at $\sqrt{s} = 13$ TeV*, *Phys. Rev. Lett.* **124** (2020) 202001 [arXiv:1911.03800] [INSPIRE].

[25] CMS collaboration, *Measurement of the differential $t\bar{t}$ production cross section as a function of the jet mass and extraction of the top quark mass in hadronic decays of boosted top quarks*, *Eur. Phys. J. C* **83** (2023) 560 [arXiv:2211.01456] [INSPIRE].

[26] ATLAS collaboration, *Measurement of the jet mass in high transverse momentum $Z(\to b\bar{b})\gamma$ production at $\sqrt{s} = 13$ TeV using the ATLAS detector*, *Phys. Lett. B* **812** (2021) 135991 [arXiv:1907.07093] [INSPIRE].

[27] CMS collaboration, *Development of the CMS detector for the CERN LHC run 3*, 2024 *JINST* **19** P05064 [arXiv:2309.05466] [INSPIRE].

[28] CMS collaboration, *Description and performance of track and primary-vertex reconstruction with the CMS tracker*, 2014 *JINST* **9** P10009 [arXiv:1405.6569] [INSPIRE].

[29] CMS Tracker Group collaboration, *The CMS phase-1 pixel detector upgrade*, 2021 *JINST* **16** P02027 [arXiv:2012.14304] [INSPIRE].

[30] CMS collaboration, *Track impact parameter resolution for the full pseudo rapidity coverage in the 2017 dataset with the CMS Phase-1 pixel detector*, CMS-DP-2020-049, CERN, Geneva, Switzerland (2020).

[31] CMS collaboration, *2017 tracking performance plots*, CMS-DP-2017-015, CERN, Geneva, Switzerland (2017).

[32] CMS collaboration, *Performance of the CMS Level-1 trigger in proton-proton collisions at $\sqrt{s} = 13$ TeV*, 2020 *JINST* **15** P10017 [arXiv:2006.10165] [INSPIRE].

[33] CMS collaboration, *The CMS trigger system*, 2017 *JINST* **12** P01020 [arXiv:1609.02366] [INSPIRE].

JHEP07(2026)054

[34] CMS collaboration, *Performance of the CMS high-level trigger during LHC Run 2*, 2024 *JINST* **19** P11021 [arXiv:2410.17038] [INSPIRE].

[35] CMS collaboration, *Particle-flow reconstruction and global event description with the CMS detector*, 2017 *JINST* **12** P10003 [arXiv:1706.04965] [INSPIRE].

[36] D. Contardo et al., *Technical proposal for the phase-II upgrade of the CMS detector*, CERN-LHCC-2015-010 (2015) [DOI:10.17181/CERN.VU8I.D59J] [INSPIRE].

[37] CMS collaboration, *Electron and photon reconstruction and identification with the CMS experiment at the CERN LHC*, 2021 *JINST* **16** P05014 [arXiv:2012.06888] [INSPIRE].

[38] CMS collaboration, *Pileup mitigation at CMS in 13 TeV data*, 2020 *JINST* **15** P09018 [arXiv:2003.00503] [INSPIRE].

[39] D. Bertolini, P. Harris, M. Low and N. Tran, *Pileup per particle identification*, *JHEP* **10** (2014) 059 [arXiv:1407.6013] [INSPIRE].

[40] M. Cacciari, G.P. Salam and G. Soyez, *The anti-k_t jet clustering algorithm*, *JHEP* **04** (2008) 063 [arXiv:0802.1189] [INSPIRE].

[41] M. Cacciari, G.P. Salam and G. Soyez, *FastJet user manual*, *Eur. Phys. J. C* **72** (2012) 1896 [arXiv:1111.6097] [INSPIRE].

[42] CMS collaboration, *Jet energy scale and resolution in the CMS experiment in pp collisions at 8 TeV*, 2017 *JINST* **12** P02014 [arXiv:1607.03663] [INSPIRE].

[43] J. Alwall et al., *The automated computation of tree-level and next-to-leading order differential cross sections, and their matching to parton shower simulations*, *JHEP* **07** (2014) 079 [arXiv:1405.0301] [INSPIRE].

[44] C. Bierlich et al., *A comprehensive guide to the physics and usage of PYTHIA 8.3*, *SciPost Phys. Codeb.* **2022** (2022) 8 [arXiv:2203.11601] [INSPIRE].

[45] CMS collaboration, *Extraction and validation of a new set of CMS PYTHIA8 tunes from underlying-event measurements*, *Eur. Phys. J. C* **80** (2020) 4 [arXiv:1903.12179] [INSPIRE].

[46] B. Andersson, G. Gustafson, G. Ingelman and T. Sjöstrand, *Parton fragmentation and string dynamics*, *Phys. Rept.* **97** (1983) 31 [INSPIRE].

[47] T. Sjöstrand, *The merging of jets*, *Phys. Lett. B* **142** (1984) 420 [INSPIRE].

[48] J. Alwall et al., *Comparative study of various algorithms for the merging of parton showers and matrix elements in hadronic collisions*, *Eur. Phys. J. C* **53** (2008) 473 [arXiv:0706.2569] [INSPIRE].

[49] J. Bellm et al., *Herwig 7.0/Herwig++ 3.0 release note*, *Eur. Phys. J. C* **76** (2016) 196 [arXiv:1512.01178] [INSPIRE].

[50] CMS collaboration, *Development and validation of HERWIG 7 tunes from CMS underlying-event measurements*, *Eur. Phys. J. C* **81** (2021) 312 [arXiv:2011.03422] [INSPIRE].

[51] R. Frederix and S. Frixione, *Merging meets matching in MC@NLO*, *JHEP* **12** (2012) 061 [arXiv:1209.6215] [INSPIRE].

[52] P. Nason, *A new method for combining NLO QCD with shower Monte Carlo algorithms*, *JHEP* **11** (2004) 040 [hep-ph/0409146] [INSPIRE].

[53] S. Frixione, P. Nason and C. Oleari, *Matching NLO QCD computations with parton shower simulations: the POWHEG method*, *JHEP* **11** (2007) 070 [arXiv:0709.2092] [INSPIRE].

JHEP07(2026)054

[54] S. Alioli, P. Nason, C. Oleari and E. Re, *A general framework for implementing NLO calculations in shower Monte Carlo programs: the POWHEG BOX*, *JHEP* **06** (2010) 043 [arXiv:1002.2581] [INSPIRE].

[55] S. Frixione, P. Nason and G. Ridolfi, *A positive-weight next-to-leading-order Monte Carlo for heavy flavour hadroproduction*, *JHEP* **09** (2007) 126 [arXiv:0707.3088] [INSPIRE].

[56] NNPDF collaboration, *Parton distributions from high-precision collider data*, *Eur. Phys. J. C* **77** (2017) 663 [arXiv:1706.00428] [INSPIRE].

[57] GEANT4 collaboration, *GEANT4 — a simulation toolkit*, *Nucl. Instrum. Meth. A* **506** (2003) 250 [INSPIRE].

[58] CMS collaboration, *Search for Higgs boson and observation of Z boson through their decay into a charm quark-antiquark pair in boosted topologies in proton-proton collisions at $\sqrt{s} = 13$ TeV*, *Phys. Rev. Lett.* **131** (2023) 041801 [arXiv:2211.14181] [INSPIRE].

[59] J.M. Lindert et al., *Precise predictions for V+jets dark matter backgrounds*, *Eur. Phys. J. C* **77** (2017) 829 [arXiv:1705.04664] [INSPIRE].

[60] CMS collaboration, *Measurement of normalized differential $t\bar{t}$ cross sections in the dilepton channel from pp collisions at $\sqrt{s} = 13$ TeV*, *JHEP* **04** (2018) 060 [arXiv:1708.07638] [INSPIRE].

[61] CMS collaboration, *Measurement of differential cross sections for top quark pair production using the lepton+jets final state in proton-proton collisions at 13 TeV*, *Phys. Rev. D* **95** (2017) 092001 [arXiv:1610.04191] [INSPIRE].

[62] Y.L. Dokshitzer, G.D. Leder, S. Moretti and B.R. Webber, *Better jet clustering algorithms*, *JHEP* **08** (1997) 001 [hep-ph/9707323] [INSPIRE].

[63] CMS collaboration, *Identification of heavy, energetic, hadronically decaying particles using machine-learning techniques*, 2020 *JINST* **15** P06005 [arXiv:2004.08262] [INSPIRE].

[64] I. Moult, L. Necib and J. Thaler, *New angles on energy correlation functions*, *JHEP* **12** (2016) 153 [arXiv:1609.07483] [INSPIRE].

[65] A.J. Larkoski, G.P. Salam and J. Thaler, *Energy correlation functions for jet substructure*, *JHEP* **06** (2013) 108 [arXiv:1305.0007] [INSPIRE].

[66] H. Qu and L. Gouskos, *ParticleNet: jet tagging via particle clouds*, *Phys. Rev. D* **101** (2020) 056019 [arXiv:1902.08570] [INSPIRE].

[67] Y. Wang et al., *Dynamic graph CNN for learning on point clouds*, *ACM Trans. Graphics* **38** (2019) 1 [arXiv:1801.07829] [INSPIRE].

[68] CMS collaboration, *Identification of highly Lorentz-boosted heavy particles using graph neural networks and new mass decorrelation techniques*, CMS-DP-2020-002, CERN, Geneva, Switzerland (2020).

[69] J. Dolen et al., *Thinking outside the ROCs: Designing Decorrelated Taggers (DDT) for jet substructure*, *JHEP* **05** (2016) 156 [arXiv:1603.00027] [INSPIRE].

[70] CMS collaboration, *Search for low mass vector resonances decaying into quark-antiquark pairs in proton-proton collisions at $\sqrt{s} = 13$ TeV*, *Phys. Rev. D* **100** (2019) 112007 [arXiv:1909.04114] [INSPIRE].

[71] CMS collaboration, *Performance of the CMS muon detector and muon reconstruction with proton-proton collisions at $\sqrt{s} = 13$ TeV*, 2018 *JINST* **13** P06015 [arXiv:1804.04528] [INSPIRE].

[72] ATLAS collaboration, *Measurement of soft-drop jet observables in pp collisions with the ATLAS detector at $\sqrt{s} = 13$ TeV*, *Phys. Rev. D* **101** (2020) 052007 [arXiv:1912.09837] [INSPIRE].

[73] CMS collaboration, *The CMS statistical analysis and combination tool: Combine*, *Comput. Softw. Big Sci.* **8** (2024) 19 [arXiv:2404.06614] [INSPIRE].

[74] CMS collaboration, *Precision luminosity measurement in proton-proton collisions at $\sqrt{s} = 13$ TeV in 2015 and 2016 at CMS*, *Eur. Phys. J. C* **81** (2021) 800 [arXiv:2104.01927] [INSPIRE].

[75] CMS collaboration, *CMS luminosity measurement for the 2017 data-taking period at $\sqrt{s} = 13$ TeV*, CMS-PAS-LUM-17-004 (2018) [INSPIRE].

[76] CMS collaboration, *CMS luminosity measurement for the 2018 data-taking period at $\sqrt{s} = 13$ TeV*, CMS-PAS-LUM-18-002 (2019) [INSPIRE].

[77] CMS collaboration, *Measurement of the inelastic proton-proton cross section at $\sqrt{s} = 13$ TeV*, *JHEP* **07** (2018) 161 [arXiv:1802.02613] [INSPIRE].

[78] M. Rubin, G.P. Salam and S. Sapeta, *Giant QCD K-factors beyond NLO*, *JHEP* **09** (2010) 084 [arXiv:1006.2144] [INSPIRE].

[79] S. Schmitt, *TUnfold: an algorithm for correcting migration effects in high energy physics*, 2012 *JINST* **7** T10003 [arXiv:1205.6201] [INSPIRE].

[80] A.N. Tikhonov, *Solution of incorrectly formulated problems and the regularization method*, *Sov. Math. Dokl.* **4** (1963) 1035.

[81] *HEPData record for this analysis*, CMS-SMP-24-012 (2026).

[82] R.D. Cousins, *Generalization of chisquare goodness-of-fit test for binned data using saturated models, with application to histograms*, https://www.physics.ucla.edu/~cousins/stats/cousins_saturated.pdf (2013).

[83] D. Britzger, *The linear template fit*, *Eur. Phys. J. C* **82** (2022) 731 [arXiv:2112.01548] [INSPIRE].

[84] S. Dittmaier and M. Huber, *Radiative corrections to the neutral-current Drell-Yan process in the Standard Model and its minimal supersymmetric extension*, *JHEP* **01** (2010) 060 [arXiv:0911.2329] [INSPIRE].

JHEP07(2026)054

The CMS collaboration

A. Hayrapetyan[1], V. Makarenko[1], A. Tumasyan[1,a], W. Adam[2], J.W. Andrejkovic[2], L. Benato[2], T. Bergauer[2], M. Dragicevic[2], C. Giordano[2], P.S. Hussain[2], M. Jeitler[2,b], N. Krammer[2], A. Li[2], D. Liko[2], M. Matthewman[2], I. Mikulec[2], J. Schieck[2,b], R. Schöfbeck[2,b], D. Schwarz[2], M. Shooshtari[2], M. Sonawane[2], W. Waltenberger[2], C.-E. Wulz[2,b], T. Janssen[3], H. Kwon[3], D. Ocampo Henao[3], T. Van Laer[3], P. Van Mechelen[3], J. Bierkens[4], N. Breugelmans[4], J. D'Hondt[4], S. Dansana[4], A. De Moor[4], M. Delcourt[4], F. Heyen[4], Y. Hong[4], P. Kashko[4], S. Lowette[4], I. Makarenko[4], D. Müller[4], J. Song[4], S. Tavernier[4], M. Tytgat[4,c], G.P. Van Onsem[4], S. Van Putte[4], D. Vannerom[4], B. Bilin[5], B. Clerbaux[5], A.K. Das[5], I. De Bruyn[5], G. De Lentdecker[5], H. Evard[5], L. Favart[5], P. Gianneios[5], A. Khalilzadeh[5], F.A. Khan[5], A. Malara[5], M.A. Shahzad[5], A. Sharma[5], L. Thomas[5], M. Vanden Bemden[5], C. Vander Velde[5], P. Vanlaer[5], F. Zhang[5], M. De Coen[6], D. Dobur[6], G. Gokbulut[6], J. Knolle[6], D. Marckx[6], K. Skovpen[6], A.M. Tomaru[6], N. Van Den Bossche[6], J. van der Linden[6], J. Vandenbroeck[6], L. Wezenbeek[6], H. Aarup Petersen[7], S. Bein[7], A. Benecke[7], A. Bethani[7], G. Bruno[7], A. Cappati[7], J. De Favereau De Jeneret[7], C. Delaere[7], F. Gameiro Casalinho[7], A. Giammanco[7], A.O. Guzel[7], V. Lemaitre[7], J. Lidrych[7], P. Malek[7], P. Mastrapasqua[7], S. Turkcapar[7], G.A. Alves[8], M. Barroso Ferreira Filho[8], E. Coelho[8], C. Hensel[8], T. Menezes De Oliveira[8], C. Mora Herrera[8], P. Rebello Teles[8], M. Soeiro[8], E.J. Tonelli Manganote[8,d], A. Vilela Pereira[8,e], W.L. Aldá Júnior[9], H. Brandao Malbouisson[9], W. Carvalho[9], J. Chinellato[9,f], M. Costa Reis[9], E.M. Da Costa[9], G.G. Da Silveira[9,g], D. De Jesus Damiao[9], S. Fonseca De Souza[9], R. Gomes De Souza[9], S. S. Jesus[9], T. Laux Kuhn[9,g], M. Macedo[9], K. Mota Amarilo[9], L. Mundim[9], H. Nogima[9], J.P. Pinheiro[9], A. Santoro[9], A. Sznajder[9], M. Thiel[9], F. Torres Da Silva De Araujo[9,h], C.A. Bernardes[10,g], F. Damas[10], T.R. Fernandez Perez Tomei[10], E.M. Gregores[10], B. Lopes Da Costa[10], I. Maietto Silverio[10], P.G. Mercadante[10], S.F. Novaes[10], B. Orzari[10], Sandra S. Padula[10], V. Scheurer[10], A. Aleksandrov[11], G. Antchev[11], P. Danev[11], R. Hadjiiska[11], P. Iaydjiev[11], M. Shopova[11], G. Sultanov[11], A. Dimitrov[12], L. Litov[12], B. Pavlov[12], P. Petkov[12], A. Petrov[12], S. Keshri[13], D. Laroze[13], S. Thakur[13], W. Brooks[14], T. Cheng[15], T. Javaid[15], L. Wang[15], L. Yuan[15], Z. Hu[16], Z. Liang[16], J. Liu[16], X. Wang[16], H. Yang[16], G.M. Chen[17,i], H.S. Chen[17,i], M. Chen[17,i], Y. Chen[17], Q. Hou[17], X. Hou[17], F. Iemmi[17], C.H. Jiang[17], A. Kapoor[17,j], H. Liao[17], G. Liu[17], Z.-A. Liu[17,k], J.N. Song[17,k], S. Song[17], J. Tao[17], C. Wang[17,i], J. Wang[17], H. Zhang[17], J. Zhao[17], A. Agapitos[18], Y. Ban[18], A. Carvalho Antunes De Oliveira[18], S. Deng[18], B. Guo[18], Q. Guo[18], C. Jiang[18], A. Levin[18], C. Li[18], Q. Li[18], Y. Mao[18], S. Qian[18], S.J. Qian[18], X. Qin[18], C. Quaranta[18], X. Sun[18], D. Wang[18], J. Wang[18], M. Zhang[18], Y. Zhao[18], C. Zhou[18], S. Yang[19], Z. You[20], K. Jaffel[21], N. Lu[21], G. Bauer[22,l,m], Z. Cui[22,m], B. Li[22,n], H. Wang[22], K. Yi[22,o], J. Zhang[22], Y. Li[23], Y. Zhou[23,p], Z. Lin[24], C. Lu[24], M. Xiao[24,q], C. Avila[25], D.A. Barbosa Trujillo[25], A. Cabrera[25], C. Florez[25], J. Fraga[25], J.A. Reyes Vega[25], C. Rendón[26], M. Rodriguez[26], A.A. Ruales Barbosa[26], J.D. Ruiz Alvarez[26], N. Godinovic[27], D. Lelas[27], A. Sculac[27], M. Kovac[28], A. Petkovic[28], T. Sculac[28], P. Bargassa[29], V. Brigljevic[29], B.K. Chitroda[29], D. Ferencek[29], K. Jakovcic[29], A. Starodumov[29], T. Susa[29], A. Attikis[30], K. Christoforou[30],

JHEP07(2026)054

C. Leonidou[30], C. Nicolaou[30], L. Paizanos[30], F. Ptochos[30], P.A. Razis[30], H. Rykaczewski[30], H. Saka[30], A. Stepennov[30], M. Finger[31,†], M. Finger Jr.[31], E. Ayala[32], E. Carrera Jarrin[33], S. Khalil[34,r], E. Salama[34,s,t], A. Hussein[35], H. Mohammed[35], M. Kadastik[36], T. Lange[36], C. Nielsen[36], J. Pata[36], M. Raidal[36], N. Seeba[36], L. Tani[36], E. Brücken[37], A. Milieva[37], K. Osterberg[37], M. Voutilainen[37], F. Garcia[38], P. Inkaew[38], K.T.S. Kallonen[38], R. Kumar Verma[38], T. Lampén[38], K. Lassila-Perini[38], B. Lehtela[38], S. Lehti[38], T. Lindén[38], N.R. Mancilla Xinto[38], M. Myllymäki[38], M.m. Rantanen[38], S. Saariokari[38], N.T. Toikka[38], J. Tuominiemi[38], N. Bin Norjoharuddeen[39], H. Kirschenmann[39], P. Luukka[39], H. Petrow[39], M. Besancon[40], F. Couderc[40], M. Dejardin[40], D. Denegri[40], P. Devouge[40], J.L. Faure[40], F. Ferri[40], P. Gaigne[40], S. Ganjour[40], P. Gras[40], G. Hamel de Monchenault[40], M. Kumar[40], V. Lohezic[40], Y. Maidannyk[40], J. Malcles[40], F. Orlandi[40], L. Portales[40], S. Ronchi[40], M.Ö. Sahin[40], A. Savoy-Navarro[40,u], P. Simkina[40], M. Titov[40], M. Tornago[40], R. Amella Ranz[41], F. Beaudette[41], G. Boldrini[41], P. Busson[41], C. Charlot[41], M. Chiusi[41], T.D. Cuisset[41], O. Davignon[41], A. De Wit[41], T. Debnath[41], I.T. Ehle[41], S. Ghosh[41], A. Gilbert[41], R. Granier de Cassagnac[41], L. Kalipoliti[41], M. Manoni[41], M. Nguyen[41], S. Obraztsov[41], C. Ochando[41], R. Salerno[41], J.B. Sauvan[41], Y. Sirois[41], G. Sokmen[41], L. Urda Gómez[41], A. Zabi[41], A. Zghiche[41], J.-L. Agram[42,v], J. Andrea[42], D. Bloch[42], J.-M. Brom[42], E.C. Chabert[42], C. Collard[42], G. Coulon[42], S. Falke[42], U. Goerlach[42], R. Haeberle[42], A.-C. Le Bihan[42], M. Meena[42], O. Poncet[42], G. Saha[42], P. Vaucelle[42], A. Di Florio[43], D. Amram[44], S. Beauceron[44], B. Blancon[44], G. Boudoul[44], N. Chanon[44], D. Contardo[44], P. Depasse[44], H. El Mamouni[44], J. Fay[44], S. Gascon[44], M. Gouzevitch[44], C. Greenberg[44], G. Grenier[44], B. Ille[44], E. Jourd'Huy[44], M. Lethuillier[44], B. Massoteau[44], L. Mirabito[44], A. Purohit[44], M. Vander Donckt[44], J. Xiao[44], A. Khvedelidze[45,w], I. Lomidze[45], Z. Tsamalaidze[45,w], V. Botta[46], S. Consuegra Rodríguez[46], L. Feld[46], K. Klein[46], M. Lipinski[46], D. Meuser[46], P. Nattland[46], V. Oppenländer[46], A. Pauls[46], D. Pérez Adán[46], N. Röwert[46], M. Teroerde[46], C. Daumann[47], S. Diekmann[47], A. Dodonova[47], N. Eich[47], D. Eliseev[47], F. Engelke[47], J. Erdmann[47], M. Erdmann[47], B. Fischer[47], T. Hebbeker[47], K. Hoepfner[47], F. Ivone[47], A. Jung[47], N. Kumar[47], M.y. Lee[47], F. Mausolf[47], M. Merschmeyer[47], A. Meyer[47], F. Nowotny[47], A. Pozdnyakov[47], W. Redjeb[47], H. Reithler[47], U. Sarkar[47], V. Sarkisovi[47], A. Schmidt[47], C. Seth[47], A. Sharma[47], J.L. Spah[47], V. Vaulin[47], S. Zaleski[47], M.R. Beckers[48], C. Dziwok[48], G. Flügge[48], N. Hoeflich[48], T. Kress[48], A. Nowack[48], O. Pooth[48], A. Stahl[48], A. Zotz[48], A. Abel[49], M. Aldaya Martin[49], J. Alimena[49], S. Amoroso[49], Y. An[49], I. Andreev[49], J. Bach[49], S. Baxter[49], M. Bayatmakou[49], H. Becerril Gonzalez[49], O. Behnke[49], A. Belvedere[49], F. Blekman[49,x], K. Borras[49,y], A. Campbell[49], S. Chatterjee[49], L.X. Coll Saravia[49], G. Eckerlin[49], D. Eckstein[49], E. Gallo[49,x], A. Geiser[49], V. Guglielmi[49], M. Guthoff[49], A. Hinzmann[49], L. Jeppe[49], M. Kasemann[49], C. Kleinwort[49], R. Kogler[49], M. Komm[49], D. Krücker[49], W. Lange[49], D. Leyva Pernia[49], K.-Y. Lin[49], K. Lipka[49,z], W. Lohmann[49,aa], J. Malvaso[49], R. Mankel[49], I.-A. Melzer-Pellmann[49], M. Mendizabal Morentin[49], A.B. Meyer[49], G. Milella[49], K. Moral Figueroa[49], A. Mussgiller[49], L.P. Nair[49], J. Niedziela[49], A. Nürnberg[49], J. Park[49], E. Ranken[49], A. Raspereza[49], D. Rastorguev[49], L. Rygaard[49],

JHEP07(2026)054

M. Scham[49,ab,ac], S. Schnake[49,y], P. Schütze[49], C. Schwanenberger[49,x], D. Selivanova[49], K. Sharko[49], M. Shchedrolosiev[49], D. Stafford[49], M. Torkian[49], A. Ventura Barroso[49], R. Walsh[49], D. Wang[49], Q. Wang[49], K. Wichmann[49], L. Wiens[49,y], C. Wissing[49], Y. Yang[49], S. Zakharov[49], A. Zimermmane Castro Santos[49], S. Albrecht[50], A.R. Alves Andrade[50], M. Antonello[50], S. Bollweg[50], M. Bonanomi[50], K. El Morabit[50], Y. Fischer[50], M. Frahm[50], E. Garutti[50], A. Grohsjean[50], A.A. Guvenli[50], J. Haller[50], D. Hundhausen[50], G. Kasieczka[50], P. Keicher[50], R. Klanner[50], W. Korcari[50], T. Kramer[50], C.c. Kuo[50], F. Labe[50], J. Lange[50], A. Lobanov[50], L. Moureaux[50], K. Nikolopoulos[50], A. Paasch[50], K.J. Pena Rodriguez[50], N. Prouvost[50], B. Raciti[50], M. Rieger[50], D. Savoiu[50], P. Schleper[50], M. Schröder[50], J. Schwandt[50], M. Sommerhalder[50], H. Stadie[50], G. Steinbrück[50], R. Ward[50], B. Wiederspan[50], M. Wolf[50], S. Brommer[51], A. Brusamolino[51], E. Butz[51], Y.M. Chen[51], T. Chwalek[51], A. Dierlamm[51], G.G. Dincer[51], U. Elicabuk[51], N. Faltermann[51], M. Giffels[51], A. Gottmann[51], F. Hartmann[51,ad], M. Horzela[51], F. Hummer[51], U. Husemann[51], J. Kieseler[51], M. Klute[51], R. Kunnilan Muhammed Rafeek[51], O. Lavoryk[51], J.M. Lawhorn[51], A. Lintuluoto[51], S. Maier[51], A.A. Monsch[51], M. Mormile[51], Th. Müller[51], E. Pfeffer[51], M. Presilla[51], G. Quast[51], K. Rabbertz[51], B. Regnery[51], R. Schmieder[51], N. Shadskiy[51], I. Shvetsov[51], H.J. Simonis[51], L. Sowa[51], L. Stockmeier[51], K. Tauqeer[51], M. Toms[51], B. Topko[51], N. Trevisani[51], C. Verstege[51], T. Voigtländer[51], R.F. Von Cube[51], J. Von Den Driesch[51], M. Wassmer[51], C. Winter[51], R. Wolf[51], W.D. Zeuner[51], X. Zuo[51], G. Anagnostou[52], G. Daskalakis[52], A. Kyriakis[52], G. Melachroinos[53], Z. Painesis[53], I. Paraskevas[53], N. Saoulidou[53], K. Theofilatos[53], E. Tziaferi[53], E. Tzovara[53], K. Vellidis[53], I. Zisopoulos[53], T. Chatzistavrou[54], G. Karapostoli[54], K. Kousouris[54], E. Siamarkou[54], G. Tsipolitis[54], I. Bestintzanos[55], I. Evangelou[55], C. Foudas[55], P. Katsoulis[55], P. Kokkas[55], P.G. Kosmoglou Kioseoglou[55], N. Manthos[55], I. Papadopoulos[55], J. Strologas[55], D. Druzhkin[56], C. Hajdu[56], D. Horvath[56,ae,af], K. Márton[56], A.J. Rádl[56,ag], F. Sikler[56], V. Veszpremi[56], M. Csanád[57], K. Farkas[57], A. Fehérkuti[57,ah], M.M.A. Gadallah[57,ai], Á. Kadlecsik[57], M. León Coello[57], G. Pásztor[57], G.I. Veres[57], L. Olah[58], B. Ujvari[58], G. Bencze[59], S. Czellar[59], J. Molnar[59], Z. Szillasi[59], T. Csorgo[60,ah], F. Nemes[60,ah], T. Novak[60], I. Szanyi[60,aj], S. Bahinipati[61,ak], S. Nayak[61], R. Raturi[61], S. Bansal[62], S.B. Beri[62], V. Bhatnagar[62], G. Chaudhary[62], S. Chauhan[62], N. Dhingra[62,al], A. Kaur[62], A. Kaur[62], H. Kaur[62], M. Kaur[62], S. Kumar[62], T. Sheokand[62], J.B. Singh[62], A. Singla[62], A. Bhardwaj[63], A. Chhetri[63], B.C. Choudhary[63], A. Kumar[63], A. Kumar[63], M. Naimuddin[63], S. Phor[63], K. Ranjan[63], M.K. Saini[63], P. Palni[64], S. Acharya[65,am], B. Gomber[65], S. Mukherjee[66], S. Bhattacharya[67], S. Das Gupta[67], S. Dutta[67], S. Dutta[67], S. Sarkar[67], M.M. Ameen[68], P.K. Behera[68], S. Chatterjee[68], G. Dash[68], A. Dattamunsi[68], P. Jana[68], P. Kalbhor[68], S. Kamble[68], J.R. Komaragiri[68,an], T. Mishra[68], P.R. Pujahari[68], A.K. Sikdar[68], R.K. Singh[68], P. Verma[68], S. Verma[68], A. Vijay[68], B.K. Sirasva[69], L. Bhatt[70], S. Dugad[70], G.B. Mohanty[70], M. Shelake[70], P. Suryadevara[70], A. Bala[71], S. Banerjee[71], S. Barman[71,ao], R.M. Chatterjee[71], M. Guchait[71], Sh. Jain[71], A. Jaiswal[71], B.M. Joshi[71], S. Kumar[71], M. Maity[71,ao], G. Majumder[71], K. Mazumdar[71], S. Parolia[71], R. Saxena[71], A. Thachayath[71], D. Maity[72,ap], P. Mal[72], K. Naskar[72,ap], A. Nayak[72,ap], K. Pal[72], P. Sadangi[72], S.K. Swain[72], S. Varghese[72,ap], D. Vats[72,ap],

JHEP07(2026)054

S. Dube[73], P. Hazarika[73], B. Kansal[73], A. Laha[73], R. Sharma[73], S. Sharma[73], K.Y. Vaish[73], S. Ghosh[74], H. Bakhshiansohi[75,aq], A. Jafari[75,ar], V. Sedighzadeh Dalavi[75], M. Zeinali[75,as], S. Bashiri[76], S. Chenarani[76,at], S.M. Etesami[76], Y. Hosseini[76], M. Khakzad[76], E. Khazaie[76], M. Mohammadi Najafabadi[76], S. Tizchang[76,au], M. Felcini[77], M. Grunewald[77], M. Abbrescia[78a,78b], M. Barbieri[78a,78b], M. Buonsante[78a,78b], A. Colaleo[78a,78b], D. Creanza[78a,78c], N. De Filippis[78a,78c], M. De Palma[78a,78b], W. Elmetenawee[78a,78b,av], N. Ferrara[78a,78c], L. Fiore[78a], L. Generoso[78a,78b], L. Longo[78a], M. Louka[78a,78b], G. Maggi[78a,78c], M. Maggi[78a], I. Margjeka[78a], V. Mastrapasqua[78a,78b], S. My[78a,78b], F. Nenna[78a,78b], S. Nuzzo[78a,78b], A. Pellecchia[78a,78b], A. Pompili[78a,78b], G. Pugliese[78a,78c], R. Radogna[78a,78b], D. Ramos[78a], A. Ranieri[78a], L. Silvestris[78a], F.M. Simone[78a,78c], Ü. Sözbilir[78a], A. Stamerra[78a,78b], D. Troiano[78a,78b], R. Venditti[78a,78b], P. Verwilligen[78a], A. Zaza[78a,78b], G. Abbiendi[79a], C. Battilana[79a,79b], D. Bonacorsi[79a,79b], P. Capiluppi[79a,79b], F.R. Cavallo[79a], M. Cuffiani[79a,79b], G.M. Dallavalle[79a], T. Diotalevi[79a,79b], F. Fabbri[79a], A. Fanfani[79a,79b], R. Farinelli[79a], P. Giacomelli[79a], C. Grandi[79a], L. Guiducci[79a,79b], S. Lo Meo[79a,aw], M. Lorusso[79a,79b], L. Lunerti[79a], S. Marcellini[79a], F.L. Navarria[79a,79b], G. Paggi[79a,79b], A. Perrotta[79a], F. Primavera[79a,79b], A.M. Rossi[79a,79b], S. Rossi Tisbeni[79a,79b], T. Rovelli[79a,79b], G.P. Siroli[79a,79b], S. Costa[80a,80b,ax], A. Di Mattia[80a], A. Lapertosa[80a], R. Potenza[80a,80b], A. Tricomi[80a,80b,ax], J. Altork[81a,81b], P. Assiouras[81a], G. Barbagli[81a], G. Bardelli[81a], M. Bartolini[81a,81b], A. Calandri[81a,81b], B. Camaiani[81a,81b], A. Cassese[81a], R. Ceccarelli[81a], V. Ciulli[81a,81b], C. Civinini[81a], R. D'Alessandro[81a,81b], L. Damenti[81a,81b], E. Focardi[81a,81b], T. Kello[81a], G. Latino[81a,81b], P. Lenzi[81a,81b], M. Lizzo[81a], M. Meschini[81a], S. Paoletti[81a], A. Papanastassiou[81a,81b], G. Sguazzoni[81a], L. Viliani[81a], L. Benussi[82], S. Colafranceschi[82,ay], S. Meola[82,az], D. Piccolo[82], M. Alves Gallo Pereira[83a], F. Ferro[83a], E. Robutti[83a], S. Tosi[83a,83b], A. Benaglia[84a], F. Brivio[84a], V. Camagni[84a,84b], F. Cetorelli[84a,84b], F. De Guio[84a,84b], M.E. Dinardo[84a,84b], P. Dini[84a], S. Gennai[84a], R. Gerosa[84a,84b], A. Ghezzi[84a,84b], P. Govoni[84a,84b], L. Guzzi[84a], M.R. Kim[84a], G. Lavizzari[84a,84b], M.T. Lucchini[84a,84b], M. Malberti[84a], S. Malvezzi[84a], A. Massironi[84a], D. Menasce[84a], L. Moroni[84a], M. Paganoni[84a,84b], S. Palluotto[84a,84b], D. Pedrini[84a], A. Perego[84a,84b], G. Pizzati[84a,84b], T. Tabarelli de Fatis[84a,84b], S. Buontempo[85a], C. Di Fraia[85a,85b], F. Fabozzi[85a,85c], L. Favilla[85a,85d], A.O.M. Iorio[85a,85b], L. Lista[85a,85b,ba], P. Paolucci[85a,ad], B. Rossi[85a], P. Azzi[86a], N. Bacchetta[86a,bb], P. Bortignon[86a,86c], G. Bortolato[86a,86b], A.C.M. Bulla[86a,86c], R. Carlin[86a,86b], P. Checchia[86a], T. Dorigo[86a,bc], F. Gasparini[86a,86b], U. Gasparini[86a,86b], S. Giorgetti[86a], E. Lusiani[86a], M. Margoni[86a,86b], A.T. Meneguzzo[86a,86b], F. Montecassiano[86a], J. Pazzini[86a,86b], P. Ronchese[86a,86b], R. Rossin[86a,86b], M. Tosi[86a,86b], A. Triossi[86a,86b], S. Ventura[86a], M. Zanetti[86a,86b], P. Zotto[86a,86b], A. Zucchetta[86a,86b], G. Zumerle[86a,86b], A. Braghieri[87a], S. Calzaferri[87a,87b], P. Montagna[87a,87b], M. Pelliccioni[87a,87b], V. Re[87a], C. Riccardi[87a,87b], P. Salvini[87a], I. Vai[87a,87b], P. Vitulo[87a,87b], S. Ajmal[88a,88b], M.E. Ascioti[88a,88b], G.M. Bilei[88a,†], C. Carrivale[88a,88b], D. Ciangottini[88a,88b], L. Della Penna[88a,88b], L. Fanò[88a,88b], V. Mariani[88a,88b], M. Menichelli[88a], F. Moscatelli[88a,bd], A. Rossi[88a,88b], A. Santocchia[88a,88b], D. Spiga[88a], T. Tedeschi[88a,88b], C. Aimè[89a,89b], C.A. Alexe[89a,89c], P. Asenov[89a,89b], P. Azzurri[89a], G. Bagliesi[89a], L. Bianchini[89a,89b], T. Boccali[89a],

JHEP07(2026)054

E. Bossini[89a], D. Bruschini[89a,89c], L. Calligaris[89a,89b], R. Castaldi[89a], F. Cattafesta[89a,89c], M.A. Ciocci[89a,89d], M. Cipriani[89a,89b], R. Dell'Orso[89a], S. Donato[89a,89b], R. Forti[89a,89b], A. Giassi[89a], F. Ligabue[89a,89c], A.C. Marini[89a,89b], D. Matos Figueiredo[89a], A. Messineo[89a,89b], S. Mishra[89a], V.K. Muraleedharan Nair Bindhu[89a,89b], S. Nandan[89a], F. Palla[89a], M. Riggirello[89a,89c], A. Rizzi[89a,89b], G. Rolandi[89a,89c], S. Roy Chowdhury[89a,be], T. Sarkar[89a], A. Scribano[89a], P. Solanki[89a,89b], P. Spagnolo[89a], F. Tenchini[89a,89b], R. Tenchini[89a], G. Tonelli[89a,89b], N. Turini[89a,89d], F. Vaselli[89a,89c], A. Venturi[89a], P.G. Verdini[89a], P. Akrap[90a,90b], C. Basile[90a,90b], S.C. Behera[90a], F. Cavallari[90a], L. Cunqueiro Mendez[90a,90b], F. De Riggi[90a,90b], D. Del Re[90a,90b], E. Di Marco[90a], M. Diemoz[90a], F. Errico[90a], L. Frosina[90a,90b], R. Gargiulo[90a,90b], B. Harikrishnan[90a,90b], F. Lombardi[90a,90b], E. Longo[90a,90b], L. Martikainen[90a,90b], J. Mijuskovic[90a,90b], G. Organtini[90a,90b], N. Palmeri[90a,90b], R. Paramatti[90a,90b], S. Rahatlou[90a,90b], C. Rovelli[90a], F. Santanastasio[90a,90b], L. Soffi[90a], V. Vladimirov[90a,90b], N. Amapane[91a,91b], R. Arcidiacono[91a,91c], S. Argiro[91a,91b], M. Arneodo[91a,91c,†], N. Bartosik[91a,91c], R. Bellan[91a,91b], A. Bellora[91a,91b], C. Biino[91a], C. Borca[91a,91b], N. Cartiglia[91a], M. Costa[91a,91b], R. Covarelli[91a,91b], N. Demaria[91a], L. Finco[91a], M. Grippo[91a,91b], B. Kiani[91a,91b], L. Lanteri[91a,91b], F. Legger[91a], F. Luongo[91a,91b], C. Mariotti[91a], S. Maselli[91a], A. Mecca[91a,91b], L. Menzio[91a,91b], P. Meridiani[91a], E. Migliore[91a,91b], M. Monteno[91a], M.M. Obertino[91a,91b], G. Ortona[91a], L. Pacher[91a,91b], N. Pastrone[91a], M. Ruspa[91a,91c], F. Siviero[91a,91b], V. Sola[91a,91b], A. Solano[91a,91b], A. Staiano[91a], C. Tarricone[91a,91b], D. Trocino[91a], G. Umoret[91a,91b], E. Vlasov[91a,91b], R. White[91a,91b], J. Babbar[92a,92b], S. Belforte[92a], V. Candelise[92a,92b], M. Casarsa[92a], F. Cossutti[92a], K. De Leo[92a], G. Della Ricca[92a,92b], R. Delli Gatti[92a,92b], S. Dogra[93], J. Hong[93], J. Kim[93], T. Kim[93], D. Lee[93], H. Lee[93], J. Lee[93], S.W. Lee[93], C.S. Moon[93], Y.D. Oh[93], S. Sekmen[93], B. Tae[93], Y.C. Yang[93], M.S. Kim[94], G. Bak[95], P. Gwak[95], H. Kim[95], D.H. Moon[95], J. Seo[95], E. Asilar[96], F. Carnevali[96], J. Choi[96,bf], T.J. Kim[96], Y. Ryou[96], S. Ha[97], S. Han[97], B. Hong[97], J. Kim[97], K. Lee[97], K.S. Lee[97], S. Lee[97], J. Yoo[97], J. Goh[98], J. Shin[98], S. Yang[98], Y. Kang[99], H. S. Kim[99], Y. Kim[99], S. Lee[99], J. Almond[100], J.H. Bhyun[100], J. Choi[100], J. Choi[100], W. Jun[100], H. Kim[100], J. Kim[100], T. Kim[100], Y. Kim[100], Y.W. Kim[100], S. Ko[100], H. Lee[100], J. Lee[100], J. Lee[100], B.H. Oh[100], S.B. Oh[100], J. Shin[100], U.K. Yang[100], I. Yoon[100], W. Jang[101], D.Y. Kang[101], D. Kim[101], S. Kim[101], B. Ko[101], J.S.H. Lee[101], Y. Lee[101], I.C. Park[101], Y. Roh[101], I.J. Watson[101], G. Cho[102], K. Hwang[102], B. Kim[102], S. Kim[102], K. Lee[102], H.D. Yoo[102], Y. Lee[103], I. Yu[103], T. Beyrouthy[104], Y. Gharbia[104], F. Alazemi[105], K. Dreimanis[106], O.M. Eberlins[106], A. Gaile[106], C. Munoz Diaz[106], D. Osite[106], G. Pikurs[106], R. Plese[106], A. Potrebko[106], M. Seidel[106], D. Sidiropoulos Kontos[106], N.R. Strautnieks[107], M. Ambrozas[108], A. Juodagalvis[108], S. Nargelas[108], A. Rinkevicius[108], G. Tamulaitis[108], I. Yusuff[109,bg], Z. Zolkapli[109], J.F. Benitez[110], A. Castaneda Hernandez[110], A. Cota Rodriguez[110], L.E. Cuevas Picos[110], H.A. Encinas Acosta[110], L.G. Gallegos Maríñez[110], J.A. Murillo Quijada[110], L. Valencia Palomo[110], G. Ayala[111], H. Castilla-Valdez[111], H. Crotte Ledesma[111], R. Lopez-Fernandez[111], J. Mejia Guisao[111], R. Reyes-Almanza[111], A. Sánchez Hernández[111], C. Oropeza Barrera[112], M. Ramírez García[112], D.L. Ramirez Guadarrama[112], I. Bautista[113],

JHEP07(2026)054

F.E. Neri Huerta[113], I. Pedraza[113], H.A. Salazar Ibarguen[113], C. Uribe Estrada[113],
I. Bubanja[114], N. Raicevic[114], P.H. Butler[115], A. Ahmad[116], M.I. Asghar[116],
A. Awais[116], M.I.M. Awan[116], W.A. Khan[116], V. Avati[117], L. Forthomme[117], L. Grzanka[117],
M. Malawski[117], K. Piotrzkowski[117], M. Bluj[118], M. Górski[118], M. Kazana[118],
M. Szleper[118], P. Zalewski[118], K. Bunkowski[119], K. Doroba[119], A. Kalinowski[119],
M. Konecki[119], J. Krolikowski[119], A. Muhammad[119], P. Fokow[120], K. Pozniak[120],
W. Zabolotny[120], M. Araujo[121], D. Bastos[121], C. Beirão Da Cruz E Silva[121], A. Boletti[121],
M. Bozzo[121], T. Camporesi[121], G. Da Molin[121], M. Gallinaro[121], J. Hollar[121],
N. Leonardo[121], G.B. Marozzo[121], A. Petrilli[121], M. Pisano[121], J. Seixas[121], J. Varela[121],
J.W. Wulff[121], P. Adzic[122], L. Markovic[122], P. Milenovic[122], V. Milosevic[122],
D. Devetak[123], M. Dordevic[123], J. Milosevic[123], L. Nadderd[123], V. Rekovic[123],
M. Stojanovic[123], M. Alcalde Martinez[124], J. Alcaraz Maestre[124], Cristina F. Bedoya[124],
J.A. Brochero Cifuentes[124], Oliver M. Carretero[124], M. Cepeda[124], M. Cerrada[124],
N. Colino[124], B. De La Cruz[124], A. Delgado Peris[124], A. Escalante Del Valle[124],
D. Fernández Del Val[124], J.P. Fernández Ramos[124], J. Flix[124], M.C. Fouz[124],
M. Gonzalez Hernandez[124], O. Gonzalez Lopez[124], S. Goy Lopez[124], J.M. Hernandez[124],
M.I. Josa[124], J. Llorente Merino[124], C. Martin Perez[124], E. Martin Viscasillas[124],
D. Moran[124], C. M. Morcillo Perez[124], Á. Navarro Tobar[124], R. Paz Herrera[124],
C. Perez Dengra[124], A. Pérez-Calero Yzquierdo[124], J. Puerta Pelayo[124], I. Redondo[124],
J. Vazquez Escobar[124], J.F. de Trocóniz[125], B. Alvarez Gonzalez[126], J. Ayllon Torresano[126],
A. Cardini[126], J. Cuevas[126], J. Del Riego Badas[126], D. Estrada Acevedo[126],
J. Fernandez Menendez[126], S. Folgueras[126], I. Gonzalez Caballero[126], P. Leguina[126],
M. Obeso Menendez[126], E. Palencia Cortezon[126], J. Prado Pico[126], A. Soto Rodríguez[126],
P. Vischia[126], S. Blanco Fernández[127], I.J. Cabrillo[127], A. Calderon[127],
J. Duarte Campderros[127], M. Fernandez[127], G. Gomez[127], C. Lasaosa García[127],
R. Lopez Ruiz[127], C. Martinez Rivero[127], P. Martinez Ruiz del Arbol[127], F. Matorras[127],
P. Matorras Cuevas[127], E. Navarrete Ramos[127], J. Piedra Gomez[127],
C. Quintana San Emeterio[127], L. Scodellaro[127], I. Vila[127], R. Vilar Cortabitarte[127],
J.M. Vizan Garcia[127], B. Kailasapathy[128,bh], D.D.C. Wickramarathna[128],
W.G.D. Dharmaratna[129,bi], K. Liyanage[129], N. Perera[129], D. Abbaneo[130], C. Amendola[130],
R. Ardino[130], E. Auffray[130], J. Baechler[130], D. Barney[130], J. Bendavid[130], M. Bianco[130],
A. Bocci[130], L. Borgonovi[130], C. Botta[130], A. Bragagnolo[130], C.E. Brown[130],
C. Caillol[130], G. Cerminara[130], P. Connor[130], D. d'Enterria[130], A. Dabrowski[130],
A. David[130], A. De Roeck[130], M.M. Defranchis[130], M. Deile[130], M. Dobson[130],
P.J. Fernández Manteca[130], B.A. Fontana Santos Alves[130], E. Fontanesi[130], W. Funk[130],
A. Gaddi[130], S. Giani[130], D. Gigi[130], K. Gill[130], F. Glege[130], M. Glowacki[130], A. Gruber[130],
J. Hegeman[130], J.K. Heikkilä[130], R. Hofsaess[130], B. Huber[130], T. James[130], P. Janot[130],
O. Kaluzinska[130], O. Karacheban[130,aa], G. Karathanasis[130], S. Laurila[130], P. Lecoq[130],
E. Leutgeb[130], C. Lourenço[130], A.-M. Lyon[130], M. Magherini[130], L. Malgeri[130],
M. Mannelli[130], A. Mehta[130], F. Meijers[130], J.A. Merlin[130], S. Mersi[130], E. Meschi[130],
M. Migliorini[130], F. Monti[130], F. Moortgat[130], M. Mulders[130], M. Musich[130],
I. Neutelings[130], S. Orfanelli[130], F. Pantaleo[130], M. Pari[130], G. Petrucciani[130],
A. Pfeiffer[130], M. Pierini[130], M. Pitt[130], H. Qu[130], D. Rabady[130], A. Reimers[130],

B. Ribeiro Lopes[130], F. Riti[130], P. Rosado[130], M. Rovere[130], H. Sakulin[130], R. Salvatico[130], S. Sanchez Cruz[130], S. Scarfi[130], M. Selvaggi[130], K. Shchelina[130], P. Silva[130], P. Sphicas[130,bj], A.G. Stahl Leiton[130], A. Steen[130], S. Summers[130], D. Treille[130], P. Tropea[130], E. Vernazza[130], J. Wanczyk[130,bk], S. Wuchterl[130], M. Zarucki[130], P. Zehetner[130], P. Zejdl[130], G. Zevi Della Porta[130], T. Bevilacqua[131,bl], L. Caminada[131,bl], W. Erdmann[131], R. Horisberger[131], Q. Ingram[131], H.C. Kaestli[131], D. Kotlinski[131], C. Lange[131], U. Langenegger[131], A. Nigamova[131], L. Noehte[131,bl], T. Rohe[131], A. Samalan[131], T.K. Aarrestad[132], M. Backhaus[132], G. Bonomelli[132], C. Cazzaniga[132], K. Datta[132], P. De Bryas Dexmiers D'Archiacchiac[132,bk], A. De Cosa[132], G. Dissertori[132], M. Dittmar[132], M. Donegà[132], F. Eble[132], K. Gedia[132], F. Glessgen[132], C. Grab[132], N. Härringer[132], T.G. Harte[132], W. Lustermann[132], M. Malucchi[132], R.A. Manzoni[132], L. Marchese[132], A. Mascellani[132,bk], F. Nessi-Tedaldi[132], F. Pauss[132], V. Perovic[132], B. Ristic[132], R. Seidita[132], J. Steggemann[132,bk], A. Tarabini[132], D. Valsecchi[132], R. Wallny[132], C. Amsler[133,bm], P. Bärtschi[133], F. Bilandzija[133], M.F. Canelli[133], G. Celotto[133], K. Cormier[133], M. Huwiler[133], A. Jofrehei[133], B. Kilminster[133], T.H. Kwok[133], S. Leontsinis[133], V. Lukashenko[133], A. Macchiolo[133], F. Meng[133], M. Missiroli[133], J. Motta[133], P. Robmann[133], E. Shokr[133], F. Stäger[133], R. Tramontano[133], P. Viscone[133], D. Bhowmik[134], C.M. Kuo[134], P.K. Rout[134], S. Taj[134], P.C. Tiwari[134,an], L. Ceard[135], K.F. Chen[135], Z.g. Chen[135], A. De Iorio[135], W.-S. Hou[135], T.h. Hsu[135], Y.w. Kao[135], S. Karmakar[135], G. Kole[135], Y.y. Li[135], R.-S. Lu[135], E. Paganis[135], X.f. Su[135], J. Thomas-Wilsker[135], L.s. Tsai[135], D. Tsionou[135], H.y. Wu[135], E. Yazgan[135], C. Asawatangtrakuldee[136], N. Srimanobhas[136], Y. Maghrbi[137], D. Agyel[138], F. Dolek[138], I. Dumanoglu[138,bn], Y. Guler[138,bo], E. Gurpinar Guler[138,bo], C. Isik[138], O. Kara[138], A. Kayis Topaksu[138], Y. Komurcu[138], G. Onengut[138], K. Ozdemir[138,bp], B. Tali[138,bq], U.G. Tok[138], E. Uslan[138], I.S. Zorbakir[138], S. Sen[139], M. Yalvac[140,br], B. Akgun[141], I.O. Atakisi[141,bs], E. Gülmez[141], M. Kaya[141,bt], O. Kaya[141,bu], M.A. Sarkisla[141,bv], S. Tekten[141,bw], D. Boncukcu[142], A. Cakir[142], K. Cankocak[142,bn,bx], B. Hacisahinoglu[143], I. Hos[143,by], B. Kaynak[143], S. Ozkorucuklu[143], O. Potok[143], H. Sert[143], C. Simsek[143], C. Zorbilmez[143], S. Cerci[144], C. Dozen[144,bz], B. Isildak[144,ca], E. Simsek[144], D. Sunar Cerci[144], T. Yetkin[144,bz], A. Boyaryntsev[145], O. Dadazhanova[145], B. Grynyov[145], L. Levchuk[146], J.J. Brooke[147], A. Bundock[147], F. Bury[147], E. Clement[147], D. Cussans[147], D. Dharmender[147], H. Flacher[147], J. Goldstein[147], H.F. Heath[147], M.-L. Holmberg[147], L. Kreczko[147], S. Paramesvaran[147], L. Robertshaw[147], M.S. Sanjrani[147,aq], J. Segal[147], V.J. Smith[147], A.H. Ball[148], K.W. Bell[148], A. Belyaev[148,cb], C. Brew[148], R.M. Brown[148], D.J.A. Cockerill[148], A. Elliot[148], K.V. Ellis[148], J. Gajownik[148], K. Harder[148], S. Harper[148], J. Linacre[148], K. Manolopoulos[148], M. Moallemi[148], D.M. Newbold[148], E. Olaiya[148], D. Petyt[148], T. Reis[148], A.R. Sahasransu[148], G. Salvi[148], T. Schuh[148], C.H. Shepherd-Themistocleous[148], I.R. Tomalin[148], K.C. Whalen[148], T. Williams[148], I. Andreou[149], R. Bainbridge[149], P. Bloch[149], O. Buchmuller[149], C.A. Carrillo Montoya[149], D. Colling[149], I. Das[149], P. Dauncey[149], G. Davies[149], M. Della Negra[149], S. Fayer[149], G. Fedi[149], G. Hall[149], H.R. Hoorani[149], A. Howard[149], G. Iles[149], C.R. Knight[149], P. Krueper[149], J. Langford[149], K.H. Law[149], J. León Holgado[149], L. Lyons[149], A.-M. Magnan[149], B. Maier[149],

S. Mallios[149], A. Mastronikolis[149], M. Mieskolainen[149], J. Nash[149,cc], M. Pesaresi[149], P.B. Pradeep[149], B.C. Radburn-Smith[149], A. Richards[149], A. Rose[149], L. Russell[149], K. Savva[149], C. Seez[149], R. Shukla[149], A. Tapper[149], K. Uchida[149], G.P. Uttley[149], T. Virdee[149,ad], M. Vojinovic[149], N. Wardle[149], D. Winterbottom[149], J.E. Cole[150], A. Khan[150], P. Kyberd[150], I.D. Reid[150], S. Abdullin[151], A. Brinkerhoff[151], E. Collins[151], M.R. Darwish[151], J. Dittmann[151], K. Hatakeyama[151], V. Hegde[151], J. Hiltbrand[151], B. McMaster[151], J. Samudio[151], S. Sawant[151], C. Sutantawibul[151], J. Wilson[151], J.M. Hogan[152], R. Bartek[153], A. Dominguez[153], S. Raj[153], B. Sahu[153,am], A.E. Simsek[153], S.S. Yu[153], B. Bam[154], A. Buchot Perraguin[154], S. Campbell[154], R. Chudasama[154], S.I. Cooper[154], C. Crovella[154], G. Fidalgo[154], S.V. Gleyzer[154], A. Khukhunaishvili[154], K. Matchev[154], E. Pearson[154], C.U. Perez[154], P. Rumerio[154,cd], E. Usai[154], R. Yi[154], S. Cholak[155], G. De Castro[155], Z. Demiragli[155], C. Erice[155], C. Fangmeier[155], C. Fernandez Madrazo[155], J. Fulcher[155], F. Golf[155], S. Jeon[155], J. O'Cain[155], I. Reed[155], J. Rohlf[155], K. Salyer[155], D. Sperka[155], D. Spitzbart[155], I. Suarez[155], A. Tsatsos[155], E. Wurtz[155], A.G. Zecchinelli[155], G. Barone[156], G. Benelli[156], D. Cutts[156], S. Ellis[156], L. Gouskos[156], M. Hadley[156], U. Heintz[156], K.W. Ho[156], T. Kwon[156], L. Lambrecht[156], G. Landsberg[156], K.T. Lau[156], J. Luo[156], S. Mondal[156], J. Roloff[156], T. Russell[156], S. Sagir[156,ce], X. Shen[156], M. Stamenkovic[156], N. Venkatasubramanian[156], S. Abbott[157], S. Baradia[157], B. Barton[157], R. Breedon[157], H. Cai[157], M. Calderon De La Barca Sanchez[157], E. Cannaert[157], M. Chertok[157], M. Citron[157], J. Conway[157], P.T. Cox[157], R. Erbacher[157], O. Kukral[157], G. Mocellin[157], S. Ostrom[157], I. Salazar Segovia[157], J.S. Tafoya Vargas[157], W. Wei[157], S. Yoo[157], K. Adamidis[158], M. Bachtis[158], D. Campos[158], R. Cousins[158], S. Crossley[158], G. Flores Avila[158], J. Hauser[158], M. Ignatenko[158], M.A. Iqbal[158], T. Lam[158], Y.f. Lo[158], E. Manca[158], A. Nunez Del Prado[158], D. Saltzberg[158], V. Valuev[158], R. Clare[159], J.W. Gary[159], G. Hanson[159], A. Aportela[160], A. Arora[160], J.G. Branson[160], S. Cittolin[160], S. Cooperstein[160], B. D'Anzi[160], D. Diaz[160], J. Duarte[160], L. Giannini[160], Y. Gu[160], J. Guiang[160], V. Krutelyov[160], R. Lee[160], J. Letts[160], H. Li[160], M. Masciovecchio[160], F. Mokhtar[160], S. Mukherjee[160], M. Pieri[160], D. Primosch[160], M. Quinnan[160], V. Sharma[160], M. Tadel[160], E. Vourliotis[160], F. Würthwein[160], A. Yagil[160], Z. Zhao[160], A. Barzdukas[161], L. Brennan[161], C. Campagnari[161], S. Carron Montero[161,cf], K. Downham[161], C. Grieco[161], M.M. Hussain[161], J. Incandela[161], M.W.K. Lai[161], A.J. Li[161], P. Masterson[161], J. Richman[161], S.N. Santpur[161], U. Sarica[161], R. Schmitz[161], D. Stuart[161], T.Á. Vámi[161], X. Yan[161], D. Zhang[161], A. Albert[162], S. Bhattacharya[162], A. Bornheim[162], O. Cerri[162], R. Kansal[162], J. Mao[162], H.B. Newman[162], G. Reales Gutiérrez[162], T. Sievert[162], M. Spiropulu[162], J.R. Vlimant[162], R.A. Wynne[162], S. Xie[162], J. Alison[163], S. An[163], M. Cremonesi[163], V. Dutta[163], E.Y. Ertorer[163], T. Ferguson[163], T.A. Gómez Espinosa[163], A. Harilal[163], A. Kallil Tharayil[163], M. Kanemura[163], C. Liu[163], M. Marchegiani[163], P. Meiring[163], S. Murthy[163], P. Palit[163], K. Park[163], M. Paulini[163], A. Roberts[163], A. Sanchez[163], W. Terrill[163], J.P. Cumalat[164], W.T. Ford[164], A. Hart[164], S. Kwan[164], J. Pearkes[164], C. Savard[164], N. Schonbeck[164], K. Stenson[164], K.A. Ulmer[164], S.R. Wagner[164], N. Zipper[164], D. Zuolo[164], J. Alexander[165], X. Chen[165], J. Dickinson[165], A. Duquette[165],

J. Fan[165], X. Fan[165], J. Grassi[165], S. Hogan[165], P. Kotamnives[165], J. Monroy[165], G. Niendorf[165], M. Oshiro[165], J.R. Patterson[165], A. Ryd[165], J. Thom[165], P. Wittich[165], R. Zou[165], L. Zygala[165], M. Albrow[166], M. Alyari[166], O. Amram[166], G. Apollinari[166], A. Apresyan[166], L.A.T. Bauerdick[166], D. Berry[166], J. Berryhill[166], P.C. Bhat[166], K. Burkett[166], J.N. Butler[166], A. Canepa[166], G.B. Cerati[166], H.W.K. Cheung[166], F. Chlebana[166], C. Cosby[166], G. Cummings[166], I. Dutta[166], V.D. Elvira[166], J. Freeman[166], A. Gandrakota[166], Z. Gecse[166], L. Gray[166], D. Green[166], A. Grummer[166], S. Grünendahl[166], D. Guerrero[166], O. Gutsche[166], R.M. Harris[166], T.C. Herwig[166], J. Hirschauer[166], V. Innocente[166], B. Jayatilaka[166], S. Jindariani[166], M. Johnson[166], U. Joshi[166], B. Klima[166], K.H.M. Kwok[166], S. Lammel[166], C. Lee[166], D. Lincoln[166], R. Lipton[166], T. Liu[166], K. Maeshima[166], D. Mason[166], P. McBride[166], P. Merkel[166], S. Mrenna[166], S. Nahn[166], J. Ngadiuba[166], D. Noonan[166], S. Norberg[166], V. Papadimitriou[166], N. Pastika[166], K. Pedro[166], C. Pena[166,cg], C.E. Perez Lara[166], F. Ravera[166], A. Reinsvold Hall[166,ch], L. Ristori[166], M. Safdari[166], E. Sexton-Kennedy[166], N. Smith[166], A. Soha[166], L. Spiegel[166], S. Stoynev[166], J. Strait[166], L. Taylor[166], S. Tkaczyk[166], N.V. Tran[166], L. Uplegger[166], E.W. Vaandering[166], C. Wang[166], I. Zoi[166], C. Aruta[167], P. Avery[167], D. Bourilkov[167], P. Chang[167], V. Cherepanov[167], R.D. Field[167], C. Huh[167], E. Koenig[167], M. Kolosova[167], J. Konigsberg[167], A. Korytov[167], G. Mitselmakher[167], K. Mohrman[167], A. Muthirakalayil Madhu[167], N. Rawal[167], S. Rosenzweig[167], V. Sulimov[167], Y. Takahashi[167], J. Wang[167], T. Adams[168], A. Al Kadhim[168], A. Askew[168], S. Bower[168], R. Goff[168], R. Hashmi[168], A. Hassani[168], R.S. Kim[168], T. Kolberg[168], G. Martinez[168], M. Mazza[168], H. Prosper[168], P.R. Prova[168], R. Yohay[168], B. Alsufyani[169], S. Butalla[169], S. Das[169], M. Hohlmann[169], M. Lavinsky[169], E. Yanes[169], M.R. Adams[170], N. Barnett[170], A. Baty[170], C. Bennett[170], R. Cavanaugh[170], R. Escobar Franco[170], O. Evdokimov[170], C.E. Gerber[170], H. Gupta[170], M. Hawksworth[170], A. Hingrajiya[170], D.J. Hofman[170], Z. Huang[170], J.h. Lee[170], C. Mills[170], S. Nanda[170], G. Nigmatkulov[170], B. Ozek[170], T. Phan[170], D. Pilipovic[170], R. Pradhan[170], E. Prifti[170], P. Roy[170], T. Roy[170], D. Shekar[170], N. Singh[170], M.B. Tonjes[170], N. Varelas[170], M.A. Wadud[170], J. Yoo[170], M. Alhusseini[171], D. Blend[171], K. Dilsiz[171,ci], O.K. Köseyan[171], A. Mestvirishvili[171,cj], O. Neogi[171], H. Ogul[171,ck], Y. Onel[171], A. Penzo[171], C. Snyder[171], E. Tiras[171,cl], B. Blumenfeld[172], J. Davis[172], A.V. Gritsan[172], L. Kang[172], S. Kyriacou[172], P. Maksimovic[172], M. Roguljic[172], S. Sekhar[172], M.V. Srivastav[172], M. Swartz[172], A. Abreu[173], L.F. Alcerro Alcerro[173], J. Anguiano[173], S. Arteaga Escatel[173], P. Baringer[173], A. Bean[173], R. Bhattacharya[173], Z. Flowers[173], D. Grove[173], J. King[173], G. Krintiras[173], M. Lazarovits[173], C. Le Mahieu[173], J. Marquez[173], M. Murray[173], M. Nickel[173], S. Popescu[173,cm], C. Rogan[173], C. Royon[173], S. Rudrabhatla[173], S. Sanders[173], C. Smith[173], G. Wilson[173], B. Allmond[174], N. Islam[174], A. Ivanov[174], K. Kaadze[174], Y. Maravin[174], J. Natoli[174], G.G. Reddy[174], D. Roy[174], G. Sorrentino[174], A. Baden[175], A. Belloni[175], J. Bistany-riebman[175], S.C. Eno[175], N.J. Hadley[175], S. Jabeen[175], R.G. Kellogg[175], T. Koeth[175], B. Kronheim[175], S. Lascio[175], P. Major[175], A.C. Mignerey[175], C. Palmer[175], C. Papageorgakis[175], M.M. Paranjpe[175], E. Popova[175,cn], A. Shevelev[175], L. Zhang[175], C. Baldenegro Barrera[176], H. Bossi[176], S. Bright-Thonney[176], I.A. Cali[176], Y.c. Chen[176], P.c. Chou[176], M. D'Alfonso[176],

JHEP07(2026)054

J. Eysermans[176], C. Freer[176], G. Gomez-Ceballos[176], M. Goncharov[176], G. Grosso[176], P. Harris[176], D. Hoang[176], G.M. Innocenti[176], K. Ivanov[176], D. Kovalskyi[176], J. Krupa[176], L. Lavezzo[176], Y.-J. Lee[176], K. Long[176], C. Mcginn[176], A. Novak[176], M.I. Park[176], C. Paus[176], C. Reissel[176], C. Roland[176], G. Roland[176], S. Rothman[176], T.a. Sheng[176], G.S.F. Stephans[176], D. Walter[176], J. Wang[176], Z. Wang[176], B. Wyslouch[176], T. J. Yang[176], A. Alpana[177], B. Crossman[177], W.J. Jackson[177], C. Kapsiak[177], M. Krohn[177], D. Mahon[177], J. Mans[177], B. Marzocchi[177], R. Rusack[177], O. Sancar[177], R. Saradhy[177], N. Strobbe[177], K. Bloom[178], D.R. Claes[178], G. Haza[178], J. Hossain[178], C. Joo[178], I. Kravchenko[178], A. Rohilla[178], J.E. Siado[178], W. Tabb[178], A. Vagnerini[178], A. Wightman[178], F. Yan[178], H. Bandyopadhyay[179], L. Hay[179], H.w. Hsia[179], I. Iashvili[179], A. Kalogeropoulos[179], A. Kharchilava[179], A. Mandal[179], M. Morris[179], D. Nguyen[179], S. Rappoccio[179], H. Rejeb Sfar[179], A. Williams[179], P. Young[179], D. Yu[179], G. Alverson[180], E. Barberis[180], J. Bonilla[180], B. Bylsma[180], M. Campana[180], J. Dervan[180], Y. Haddad[180], Y. Han[180], I. Israr[180], A. Krishna[180], M. Lu[180], N. Manganelli[180], R. Mccarthy[180], D.M. Morse[180], T. Orimoto[180], L. Skinnari[180], C.S. Thoreson[180], E. Tsai[180], D. Wood[180], S. Dittmer[181], K.A. Hahn[181], M. Mcginnis[181], Y. Miao[181], D.G. Monk[181], M.H. Schmitt[181], A. Taliercio[181], M. Velasco[181], J. Wang[181], G. Agarwal[182], R. Band[182], R. Bucci[182], S. Castells[182], A. Das[182], A. Datta[182], A. Ehnis[182], R. Goldouzian[182], M. Hildreth[182], K. Hurtado Anampa[182], T. Ivanov[182], C. Jessop[182], A. Karneyeu[182], K. Lannon[182], J. Lawrence[182], N. Loukas[182], L. Lutton[182], J. Mariano[182], N. Marinelli[182], T. McCauley[182], C. Mcgrady[182], C. Moore[182], Y. Musienko[182,co], H. Nelson[182], M. Osherson[182], A. Piccinelli[182], R. Ruchti[182], A. Townsend[182], Y. Wan[182], M. Wayne[182], H. Yockey[182], A. Basnet[183], M. Carrigan[183], R. De Los Santos[183], L.S. Durkin[183], C. Hill[183], M. Joyce[183], D.A. Wenzl[183], B.L. Winer[183], B. R. Yates[183], H. Bouchamaoui[184], G. Dezoort[184], P. Elmer[184], A. Frankenthal[184], M. Galli[184], B. Greenberg[184], N. Haubrich[184], K. Kennedy[184], G. Kopp[184], Y. Lai[184], D. Lange[184], A. Loeliger[184], D. Marlow[184], I. Ojalvo[184], J. Olsen[184], F. Simpson[184], D. Stickland[184], C. Tully[184], S. Malik[185], R. Sharma[185], S. Chandra[186], R. Chawla[186], A. Gu[186], L. Gutay[186], M. Jones[186], A.W. Jung[186], D. Kondratyev[186], M. Liu[186], G. Negro[186], N. Neumeister[186], G. Paspalaki[186], S. Piperov[186], N.R. Saha[186], J.F. Schulte[186], F. Wang[186], A. Wildridge[186], W. Xie[186], Y. Yao[186], Y. Zhong[186], N. Parashar[187], A. Pathak[187], E. Shumka[187], D. Acosta[188], A. Agrawal[188], C. Arbour[188], T. Carnahan[188], P. Das[188], K.M. Ecklund[188], S. Freed[188], F.J.M. Geurts[188], T. Huang[188], I. Krommydas[188], N. Lewis[188], W. Li[188], J. Lin[188], O. Miguel Colin[188], B.P. Padley[188], R. Redjimi[188], J. Rotter[188], C. Vico Villalba[188], M. Wulansatiti[188], E. Yigitbasi[188], Y. Zhang[188], O. Bessidskaia Bylund[189], A. Bodek[189], P. de Barbaro[189,†], R. Demina[189], A. Garcia-Bellido[189], H.S. Hare[189], O. Hindrichs[189], N. Parmar[189], P. Parygin[189,cn], H. Seo[189], R. Taus[189], B. Chiarito[190], J.P. Chou[190], S.V. Clark[190], S. Donnelly[190], D. Gadkari[190], Y. Gershtein[190], E. Halkiadakis[190], C. Houghton[190], D. Jaroslawski[190], A. Kobert[190], S. Konstantinou[190], I. Laflotte[190], A. Lath[190], J. Martins[190], M. Perez Prada[190], B. Rand[190], J. Reichert[190], P. Saha[190], S. Salur[190], S. Schnetzer[190], S. Somalwar[190], R. Stone[190], S.A. Thayil[190], S. Thomas[190], J. Vora[190], D. Ally[191],

JHEP07(2026)054

A.G. Delannoy[191], S. Fiorendi[191], J. Harris[191], T. Holmes[191], A.R. Kanuganti[191], N. Karunarathna[191], J. Lawless[191], L. Lee[191], E. Nibigira[191], B. Skipworth[191], S. Spanier[191], D. Aebi[192], M. Ahmad[192], T. Akhter[192], K. Androsov[192], A. Bolshov[192], O. Bouhali[192,cp], A. Cagnotta[192], V. D'Amante[192], R. Eusebi[192], P. Flanagan[192], J. Gilmore[192], Y. Guo[192], T. Kamon[192], S. Luo[192], R. Mueller[192], A. Safonov[192], N. Akchurin[193], J. Damgov[193], Y. Feng[193], N. Gogate[193], W. Jin[193], Y. Kazhykarim[193], K. Lamichhane[193], S.W. Lee[193], C. Madrid[193], A. Mankel[193], T. Peltola[193], I. Volobouev[193], E. Appelt[194], Y. Chen[194], S. Greene[194], A. Gurrola[194], W. Johns[194], R. Kunnawalkam Elayavalli[194], A. Melo[194], D. Rathjens[194], F. Romeo[194], P. Sheldon[194], S. Tuo[194], J. Velkovska[194], J. Viinikainen[194], J. Zhang[194], B. Cardwell[195], H. Chung[195], B. Cox[195], J. Hakala[195], G. Hamilton Ilha Machado[195], R. Hirosky[195], M. Jose[195], A. Ledovskoy[195], C. Mantilla[195], C. Neu[195], C. Ramón Álvarez[195], Z. Wu[195], S. Bhattacharya[196], P.E. Karchin[196], A. Aravind[197], S. Banerjee[197], K. Black[197], T. Bose[197], E. Chavez[197], S. Dasu[197], P. Everaerts[197], C. Galloni[197], H. He[197], M. Herndon[197], A. Herve[197], C.K. Koraka[197], S. Lomte[197], R. Loveless[197], A. Mallampalli[197], A. Mohammadi[197], S. Mondal[197], T. Nelson[197], G. Parida[197], L. Pétré[197], D. Pinna[197], A. Savin[197], V. Shang[197], V. Sharma[197], W.H. Smith[197], D. Teague[197], H.F. Tsoi[197], W. Vetens[197], A. Warden[197], S. Afanasiev[198], V. Alexakhin[198], Yu. Andreev[198], T. Aushev[198], D. Budkouski[198], R. Chistov[198], M. Danilov[198], T. Dimova[198], A. Ershov[198], S. Gninenko[198], I. Gorbunov[198], A. Gribushin[198], A. Kamenev[198], V. Karjavine[198], M. Kirsanov[198], O. Kodolova[198,cq], V. Korenkov[198], I. Korsakov[198], A. Kozyrev[198], N. Krasnikov[198], A. Lanev[198], A. Malakhov[198], V. Matveev[198], A. Nikitenko[198,cr,cs], V. Palichik[198], V. Perelygin[198], S. Polikarpov[198], O. Radchenko[198], M. Savina[198], V. Shalaev[198], S. Shmatov[198], S. Shulha[198], Y. Skovpen[198], K. Slizhevskiy[198], V. Smirnov[198], O. Teryaev[198], I. Tlisova[198], A. Toropin[198], N. Voytishin[198], A. Zarubin[198], I. Zhizhin[198], E. Boos[199], V. Bunichev[199], M. Dubinin[199,cg], L. Dudko[199], V. Kim[199,co], V. Murzin[199], V. Oreshkin[199], V. Savrin[199], A. Snigirev[199], D. Sosnov[199]

[1] *Yerevan Physics Institute, Yerevan, Armenia*
[2] *Institut für Hochenergiephysik, Vienna, Austria*
[3] *Universiteit Antwerpen, Antwerpen, Belgium*
[4] *Vrije Universiteit Brussel, Brussel, Belgium*
[5] *Université Libre de Bruxelles, Bruxelles, Belgium*
[6] *Ghent University, Ghent, Belgium*
[7] *Université Catholique de Louvain, Louvain-la-Neuve, Belgium*
[8] *Centro Brasileiro de Pesquisas Fisicas, Rio de Janeiro, Brazil*
[9] *Universidade do Estado do Rio de Janeiro, Rio de Janeiro, Brazil*
[10] *Universidade Estadual Paulista, Universidade Federal do ABC, São Paulo, Brazil*
[11] *Institute for Nuclear Research and Nuclear Energy, Bulgarian Academy of Sciences, Sofia, Bulgaria*
[12] *University of Sofia, Sofia, Bulgaria*
[13] *Instituto De Alta Investigación, Universidad de Tarapacá, Casilla 7 D, Arica, Chile*
[14] *Universidad Tecnica Federico Santa Maria, Valparaiso, Chile*
[15] *Beihang University, Beijing, China*
[16] *Department of Physics, Tsinghua University, Beijing, China*
[17] *Institute of High Energy Physics, Beijing, China*
[18] *State Key Laboratory of Nuclear Physics and Technology, Peking University, Beijing, China*

[19] *State Key Laboratory of Nuclear Physics and Technology, Institute of Quantum Matter, South China Normal University, Guangzhou, China*
[20] *Sun Yat-Sen University, Guangzhou, China*
[21] *University of Science and Technology of China, Hefei, China*
[22] *Nanjing Normal University, Nanjing, China*
[23] *Institute of Modern Physics and Key Laboratory of Nuclear Physics and Ion-beam Application (MOE) — Fudan University, Shanghai, China*
[24] *Zhejiang University, Hangzhou, Zhejiang, China*
[25] *Universidad de Los Andes, Bogota, Colombia*
[26] *Universidad de Antioquia, Medellin, Colombia*
[27] *University of Split, Faculty of Electrical Engineering, Mechanical Engineering and Naval Architecture, Split, Croatia*
[28] *University of Split, Faculty of Science, Split, Croatia*
[29] *Institute Rudjer Boskovic, Zagreb, Croatia*
[30] *University of Cyprus, Nicosia, Cyprus*
[31] *Charles University, Prague, Czech Republic*
[32] *Escuela Politecnica Nacional, Quito, Ecuador*
[33] *Universidad San Francisco de Quito, Quito, Ecuador*
[34] *Academy of Scientific Research and Technology of the Arab Republic of Egypt, Egyptian Network of High Energy Physics, Cairo, Egypt*
[35] *Center for High Energy Physics (CHEP-FU), Fayoum University, El-Fayoum, Egypt*
[36] *National Institute of Chemical Physics and Biophysics, Tallinn, Estonia*
[37] *Department of Physics, University of Helsinki, Helsinki, Finland*
[38] *Helsinki Institute of Physics, Helsinki, Finland*
[39] *Lappeenranta-Lahti University of Technology, Lappeenranta, Finland*
[40] *IRFU, CEA, Université Paris-Saclay, Gif-sur-Yvette, France*
[41] *Laboratoire Leprince-Ringuet, CNRS/IN2P3, Ecole Polytechnique, Institut Polytechnique de Paris, Palaiseau, France*
[42] *Université de Strasbourg, CNRS, IPHC UMR 7178, Strasbourg, France*
[43] *Centre de Calcul de l'Institut National de Physique Nucleaire et de Physique des Particules, CNRS/IN2P3, Villeurbanne, France*
[44] *Institut de Physique des 2 Infinis de Lyon (IP2I), Villeurbanne, France*
[45] *Georgian Technical University, Tbilisi, Georgia*
[46] *RWTH Aachen University, I. Physikalisches Institut, Aachen, Germany*
[47] *RWTH Aachen University, III. Physikalisches Institut A, Aachen, Germany*
[48] *RWTH Aachen University, III. Physikalisches Institut B, Aachen, Germany*
[49] *Deutsches Elektronen-Synchrotron, Hamburg, Germany*
[50] *University of Hamburg, Hamburg, Germany*
[51] *Karlsruher Institut fuer Technologie, Karlsruhe, Germany*
[52] *Institute of Nuclear and Particle Physics (INPP), NCSR Demokritos, Aghia Paraskevi, Greece*
[53] *National and Kapodistrian University of Athens, Athens, Greece*
[54] *National Technical University of Athens, Athens, Greece*
[55] *University of Ioánnina, Ioánnina, Greece*
[56] *HUN-REN Wigner Research Centre for Physics, Budapest, Hungary*
[57] *MTA-ELTE Lendület CMS Particle and Nuclear Physics Group, Eötvös Loránd University, Budapest, Hungary*
[58] *Faculty of Informatics, University of Debrecen, Debrecen, Hungary*
[59] *HUN-REN ATOMKI — Institute of Nuclear Research, Debrecen, Hungary*
[60] *Karoly Robert Campus, MATE Institute of Technology, Gyongyos, Hungary*
[61] *IIT Bhubaneswar, Bhubaneswar, India*
[62] *Panjab University, Chandigarh, India*
[63] *University of Delhi, Delhi, India*
[64] *Indian Institute of Technology Mandi (IIT-Mandi), Himachal Pradesh, India*

JHEP07(2026)054

[65] University of Hyderabad, Hyderabad, India
[66] Indian Institute of Technology Kanpur, Kanpur, India
[67] Saha Institute of Nuclear Physics, HBNI, Kolkata, India
[68] Indian Institute of Technology Madras, Madras, India
[69] IISER Mohali, India, Mohali, India
[70] Tata Institute of Fundamental Research-A, Mumbai, India
[71] Tata Institute of Fundamental Research-B, Mumbai, India
[72] National Institute of Science Education and Research, An OCC of Homi Bhabha National Institute, Bhubaneswar, Odisha, India
[73] Indian Institute of Science Education and Research (IISER), Pune, India
[74] Indian Institute of Technology Hyderabad, Telangana, India
[75] Isfahan University of Technology, Isfahan, Iran
[76] Institute for Research in Fundamental Sciences (IPM), Tehran, Iran
[77] University College Dublin, Dublin, Ireland
[78a] INFN Sezione di Bari, Bari, Italy
[78b] Università di Bari, Bari, Italy
[78c] Politecnico di Bari, Bari, Italy
[79a] INFN Sezione di Bologna, Bologna, Italy
[79b] Università di Bologna, Bologna, Italy
[80a] INFN Sezione di Catania, Catania, Italy
[80b] Università di Catania, Catania, Italy
[81a] INFN Sezione di Firenze, Firenze, Italy
[81b] Università di Firenze, Firenze, Italy
[82] INFN Laboratori Nazionali di Frascati, Frascati, Italy
[83a] INFN Sezione di Genova, Genova, Italy
[83b] Università di Genova, Genova, Italy
[84a] INFN Sezione di Milano-Bicocca, Milano, Italy
[84b] Università di Milano-Bicocca, Milano, Italy
[85a] INFN Sezione di Napoli, Napoli, Italy
[85b] Università di Napoli 'Federico II', Napoli, Italy
[85c] Università della Basilicata, Potenza, Italy
[85d] Scuola Superiore Meridionale (SSM), Napoli, Italy
[86a] INFN Sezione di Padova, Padova, Italy
[86b] Università di Padova, Padova, Italy
[86c] Universita degli Studi di Cagliari, Cagliari, Italy
[87a] INFN Sezione di Pavia, Pavia, Italy
[87b] Università di Pavia, Pavia, Italy
[88a] INFN Sezione di Perugia, Perugia, Italy
[88b] Università di Perugia, Perugia, Italy
[89a] INFN Sezione di Pisa, Pisa, Italy
[89b] Università di Pisa, Pisa, Italy
[89c] Scuola Normale Superiore di Pisa, Pisa, Italy
[89d] Università di Siena, Siena, Italy
[90a] INFN Sezione di Roma, Roma, Italy
[90b] Sapienza Università di Roma, Roma, Italy
[91a] INFN Sezione di Torino, Torino, Italy
[91b] Università di Torino, Torino, Italy
[91c] Università del Piemonte Orientale, Novara, Italy
[92a] INFN Sezione di Trieste, Trieste, Italy
[92b] Università di Trieste, Trieste, Italy
[93] Kyungpook National University, Daegu, Korea
[94] Department of Mathematics and Physics — GWNU, Gangneung, Korea
[95] Chonnam National University, Institute for Universe and Elementary Particles, Kwangju, Korea

[96] *Hanyang University, Seoul, Korea*
[97] *Korea University, Seoul, Korea*
[98] *Kyung Hee University, Department of Physics, Seoul, Korea*
[99] *Sejong University, Seoul, Korea*
[100] *Seoul National University, Seoul, Korea*
[101] *University of Seoul, Seoul, Korea*
[102] *Yonsei University, Department of Physics, Seoul, Korea*
[103] *Sungkyunkwan University, Suwon, Korea*
[104] *College of Engineering and Technology, American University of the Middle East (AUM), Dasman, Kuwait*
[105] *Kuwait University — College of Science — Department of Physics, Safat, Kuwait*
[106] *Riga Technical University, Riga, Latvia*
[107] *University of Latvia (LU), Riga, Latvia*
[108] *Vilnius University, Vilnius, Lithuania*
[109] *National Centre for Particle Physics, Universiti Malaya, Kuala Lumpur, Malaysia*
[110] *Universidad de Sonora (UNISON), Hermosillo, Mexico*
[111] *Centro de Investigacion y de Estudios Avanzados del IPN, Mexico City, Mexico*
[112] *Universidad Iberoamericana, Mexico City, Mexico*
[113] *Benemerita Universidad Autonoma de Puebla, Puebla, Mexico*
[114] *University of Montenegro, Podgorica, Montenegro*
[115] *University of Canterbury, Christchurch, New Zealand*
[116] *National Centre for Physics, Quaid-I-Azam University, Islamabad, Pakistan*
[117] *AGH University of Krakow, Krakow, Poland*
[118] *National Centre for Nuclear Research, Swierk, Poland*
[119] *Institute of Experimental Physics, Faculty of Physics, University of Warsaw, Warsaw, Poland*
[120] *Warsaw University of Technology, Warsaw, Poland*
[121] *Laboratório de Instrumentação e Física Experimental de Partículas, Lisboa, Portugal*
[122] *Faculty of Physics, University of Belgrade, Belgrade, Serbia*
[123] *VINCA Institute of Nuclear Sciences, University of Belgrade, Belgrade, Serbia*
[124] *Centro de Investigaciones Energéticas Medioambientales y Tecnológicas (CIEMAT), Madrid, Spain*
[125] *Universidad Autónoma de Madrid, Madrid, Spain*
[126] *Universidad de Oviedo, Instituto Universitario de Ciencias y Tecnologías Espaciales de Asturias (ICTEA), Oviedo, Spain*
[127] *Instituto de Física de Cantabria (IFCA), CSIC-Universidad de Cantabria, Santander, Spain*
[128] *University of Colombo, Colombo, Sri Lanka*
[129] *University of Ruhuna, Department of Physics, Matara, Sri Lanka*
[130] *CERN, European Organization for Nuclear Research, Geneva, Switzerland*
[131] *PSI Center for Neutron and Muon Sciences, Villigen, Switzerland*
[132] *ETH Zurich — Institute for Particle Physics and Astrophysics (IPA), Zurich, Switzerland*
[133] *Universität Zürich, Zurich, Switzerland*
[134] *National Central University, Chung-Li, Taiwan*
[135] *National Taiwan University (NTU), Taipei, Taiwan*
[136] *High Energy Physics Research Unit, Department of Physics, Faculty of Science, Chulalongkorn University, Bangkok, Thailand*
[137] *Tunis El Manar University, Tunis, Tunisia*
[138] *Çukurova University, Physics Department, Science and Art Faculty, Adana, Turkey*
[139] *Hacettepe University, Ankara, Turkey*
[140] *Middle East Technical University, Physics Department, Ankara, Turkey*
[141] *Bogazici University, Istanbul, Turkey*
[142] *Istanbul Technical University, Istanbul, Turkey*
[143] *Istanbul University, Istanbul, Turkey*
[144] *Yildiz Technical University, Istanbul, Turkey*
[145] *Institute for Scintillation Materials of National Academy of Science of Ukraine, Kharkiv, Ukraine*
[146] *National Science Centre, Kharkiv Institute of Physics and Technology, Kharkiv, Ukraine*

JHEP07(2026)054

[147] *University of Bristol, Bristol, U.K.*
[148] *Rutherford Appleton Laboratory, Didcot, U.K.*
[149] *Imperial College, London, U.K.*
[150] *Brunel University, Uxbridge, U.K.*
[151] *Baylor University, Waco, Texas, U.S.A.*
[152] *Bethel University, St. Paul, Minnesota, U.S.A.*
[153] *Catholic University of America, Washington, DC, U.S.A.*
[154] *The University of Alabama, Tuscaloosa, Alabama, U.S.A.*
[155] *Boston University, Boston, Massachusetts, U.S.A.*
[156] *Brown University, Providence, Rhode Island, U.S.A.*
[157] *University of California, Davis, Davis, California, U.S.A.*
[158] *University of California, Los Angeles, California, U.S.A.*
[159] *University of California, Riverside, Riverside, California, U.S.A.*
[160] *University of California, San Diego, La Jolla, California, U.S.A.*
[161] *University of California, Santa Barbara — Department of Physics, Santa Barbara, California, U.S.A.*
[162] *California Institute of Technology, Pasadena, California, U.S.A.*
[163] *Carnegie Mellon University, Pittsburgh, Pennsylvania, U.S.A.*
[164] *University of Colorado Boulder, Boulder, Colorado, U.S.A.*
[165] *Cornell University, Ithaca, New York, U.S.A.*
[166] *Fermi National Accelerator Laboratory, Batavia, Illinois, U.S.A.*
[167] *University of Florida, Gainesville, Florida, U.S.A.*
[168] *Florida State University, Tallahassee, Florida, U.S.A.*
[169] *Florida Institute of Technology, Melbourne, Florida, U.S.A.*
[170] *University of Illinois Chicago, Chicago, Illinois, U.S.A.*
[171] *The University of Iowa, Iowa City, Iowa, U.S.A.*
[172] *Johns Hopkins University, Baltimore, Maryland, U.S.A.*
[173] *The University of Kansas, Lawrence, Kansas, U.S.A.*
[174] *Kansas State University, Manhattan, Kansas, U.S.A.*
[175] *University of Maryland, College Park, Maryland, U.S.A.*
[176] *Massachusetts Institute of Technology, Cambridge, Massachusetts, U.S.A.*
[177] *University of Minnesota, Minneapolis, Minnesota, U.S.A.*
[178] *University of Nebraska-Lincoln, Lincoln, Nebraska, U.S.A.*
[179] *State University of New York at Buffalo, Buffalo, New York, U.S.A.*
[180] *Northeastern University, Boston, Massachusetts, U.S.A.*
[181] *Northwestern University, Evanston, Illinois, U.S.A.*
[182] *University of Notre Dame, Notre Dame, Indiana, U.S.A.*
[183] *The Ohio State University, Columbus, Ohio, U.S.A.*
[184] *Princeton University, Princeton, New Jersey, U.S.A.*
[185] *University of Puerto Rico, Mayaguez, Puerto Rico, U.S.A.*
[186] *Purdue University, West Lafayette, Indiana, U.S.A.*
[187] *Purdue University Northwest, Hammond, Indiana, U.S.A.*
[188] *Rice University, Houston, Texas, U.S.A.*
[189] *University of Rochester, Rochester, New York, U.S.A.*
[190] *Rutgers, The State University of New Jersey, Piscataway, New Jersey, U.S.A.*
[191] *University of Tennessee, Knoxville, Tennessee, U.S.A.*
[192] *Texas A&M University, College Station, Texas, U.S.A.*
[193] *Texas Tech University, Lubbock, Texas, U.S.A.*
[194] *Vanderbilt University, Nashville, Tennessee, U.S.A.*
[195] *University of Virginia, Charlottesville, Virginia, U.S.A.*
[196] *Wayne State University, Detroit, Michigan, U.S.A.*
[197] *University of Wisconsin — Madison, Madison, Wisconsin, U.S.A.*
[198] *An institute or international laboratory covered by a cooperation agreement with CERN*
[199] *An institute formerly covered by a cooperation agreement with CERN*

[a] Also at Yerevan State University, Yerevan, Armenia
[b] Also at TU Wien, Vienna, Austria
[c] Also at Ghent University, Ghent, Belgium
[d] Also at FACAMP — Faculdades de Campinas, Sao Paulo, Brazil
[e] Also at Universidade do Estado do Rio de Janeiro, Rio de Janeiro, Brazil
[f] Also at Universidade Estadual de Campinas, Campinas, Brazil
[g] Also at Federal University of Rio Grande do Sul, Porto Alegre, Brazil
[h] Also at The University of the State of Amazonas, Manaus, Brazil
[i] Also at University of Chinese Academy of Sciences, Beijing, China
[j] Also at China Center of Advanced Science and Technology, Beijing, China
[k] Also at University of Chinese Academy of Sciences, Beijing, China
[l] Also at School of Physics, Zhengzhou University, Zhengzhou, China
[m] Now at Henan Normal University, Xinxiang, China
[n] Also at University of Shanghai for Science and Technology, Shanghai, China
[o] Now at The University of Iowa, Iowa City, Iowa, U.S.A.
[p] Also at Nanjing Normal University, Nanjing, China
[q] Also at Center for High Energy Physics, Peking University, Beijing, China
[r] Also at Zewail City of Science and Technology, Zewail, Egypt
[s] Also at British University in Egypt, Cairo, Egypt
[t] Now at Ain Shams University, Cairo, Egypt
[u] Also at Purdue University, West Lafayette, Indiana, U.S.A.
[v] Also at Université de Haute Alsace, Mulhouse, France
[w] Also at Another institute or international laboratory covered by a cooperation agreement with CERN
[x] Also at University of Hamburg, Hamburg, Germany
[y] Also at RWTH Aachen University, III. Physikalisches Institut A, Aachen, Germany
[z] Also at Bergische University Wuppertal (BUW), Wuppertal, Germany
[aa] Also at Brandenburg University of Technology, Cottbus, Germany
[ab] Also at Forschungszentrum Jülich, Juelich, Germany
[ac] Now at RWTH Aachen University, III. Physikalisches Institut A, Aachen, Germany
[ad] Also at CERN, European Organization for Nuclear Research, Geneva, Switzerland
[ae] Also at HUN-REN ATOMKI — Institute of Nuclear Research, Debrecen, Hungary
[af] Now at Universitatea Babes-Bolyai — Facultatea de Fizica, Cluj-Napoca, Romania
[ag] Also at MTA-ELTE Lendület CMS Particle and Nuclear Physics Group, Eötvös Loránd University, Budapest, Hungary
[ah] Also at HUN-REN Wigner Research Centre for Physics, Budapest, Hungary
[ai] Also at Physics Department, Faculty of Science, Assiut University, Assiut, Egypt
[aj] Also at The University of Kansas, Lawrence, Kansas, U.S.A.
[ak] Also at IIT Bhubaneswar, Bhubaneswar, India
[al] Also at Punjab Agricultural University, Ludhiana, India
[am] Also at University of Hyderabad, Hyderabad, India
[an] Also at Indian Institute of Science (IISc), Bangalore, India
[ao] Also at University of Visva-Bharati, Santiniketan, India
[ap] Also at Institute of Physics, Bhubaneswar, India
[aq] Also at Deutsches Elektronen-Synchrotron, Hamburg, Germany
[ar] Also at Isfahan University of Technology, Isfahan, Iran
[as] Also at Sharif University of Technology, Tehran, Iran
[at] Also at Department of Physics, University of Science and Technology of Mazandaran, Behshahr, Iran
[au] Also at Department of Physics, Faculty of Science, Arak University, ARAK, Iran
[av] Also at Helwan University, Cairo, Egypt
[aw] Also at Italian National Agency for New Technologies, Energy and Sustainable Economic Development, Bologna, Italy
[ax] Also at Centro Siciliano di Fisica Nucleare e di Struttura Della Materia, Catania, Italy
[ay] Also at James Madison University, Harrisonburg, N/A, U.S.A.

JHEP07(2026)054

[az] Also at Università degli Studi Guglielmo Marconi, Roma, Italy
[ba] Also at Scuola Superiore Meridionale, Università di Napoli 'Federico II', Napoli, Italy
[bb] Also at Fermi National Accelerator Laboratory, Batavia, Illinois, U.S.A.
[bc] Also at Lulea University of Technology, Lulea, Sweden
[bd] Also at Consiglio Nazionale delle Ricerche — Istituto Officina dei Materiali, Perugia, Italy
[be] Also at UPES — University of Petroleum and Energy Studies, Dehradun, India
[bf] Also at Institut de Physique des 2 Infinis de Lyon (IP2I), Villeurbanne, France
[bg] Also at Department of Applied Physics, Faculty of Science and Technology, Universiti Kebangsaan Malaysia, Bangi, Malaysia
[bh] Also at Trincomalee Campus, Eastern University, Sri Lanka, Nilaveli, Sri Lanka
[bi] Also at Saegis Campus, Nugegoda, Sri Lanka
[bj] Also at National and Kapodistrian University of Athens, Athens, Greece
[bk] Also at Ecole Polytechnique Fédérale Lausanne, Lausanne, Switzerland
[bl] Also at Universität Zürich, Zurich, Switzerland
[bm] Also at Stefan Meyer Institute for Subatomic Physics, Vienna, Austria
[bn] Also at Near East University, Research Center of Experimental Health Science, Mersin, Turkey
[bo] Also at Konya Technical University, Konya, Turkey
[bp] Also at Izmir Bakircay University, Izmir, Turkey
[bq] Also at Adiyaman University, Adiyaman, Turkey
[br] Also at Bozok Universitetesi Rektörlügü, Yozgat, Turkey
[bs] Also at Istanbul Sabahattin Zaim University, Istanbul, Turkey
[bt] Also at Marmara University, Istanbul, Turkey
[bu] Also at Milli Savunma University, Istanbul, Turkey
[bv] Also at Informatics and Information Security Research Center, Gebze/Kocaeli, Turkey
[bw] Also at Kafkas University, Kars, Turkey
[bx] Now at Istanbul Okan University, Istanbul, Turkey
[by] Also at Istanbul University — Cerrahpasa, Faculty of Engineering, Istanbul, Turkey
[bz] Also at Istinye University, Istanbul, Turkey
[ca] Also at Yildiz Technical University, Istanbul, Turkey
[cb] Also at School of Physics and Astronomy, University of Southampton, Southampton, U.K.
[cc] Also at Monash University, Faculty of Science, Clayton, Australia
[cd] Also at Università di Torino, Torino, Italy
[ce] Also at Karamanoğlu Mehmetbey University, Karaman, Turkey
[cf] Also at California Lutheran University, Thousand Oaks, California, U.S.A.
[cg] Also at California Institute of Technology, Pasadena, California, U.S.A.
[ch] Also at United States Naval Academy, Annapolis, Maryland, U.S.A.
[ci] Also at Bingol University, Bingol, Turkey
[cj] Also at Georgian Technical University, Tbilisi, Georgia
[ck] Also at Sinop University, Sinop, Turkey
[cl] Also at Erciyes University, Kayseri, Turkey
[cm] Also at Horia Hulubei National Institute of Physics and Nuclear Engineering (IFIN-HH), Bucharest, Romania
[cn] Now at Another institute formerly covered by a cooperation agreement with CERN
[co] Also at Another institute formerly covered by a cooperation agreement with CERN
[cp] Also at Hamad Bin Khalifa University (HBKU), Doha, Qatar
[cq] Also at Yerevan Physics Institute, Yerevan, Armenia
[cr] Also at Imperial College, London, U.K.
[cs] Now at Yerevan Physics Institute, Yerevan, Armenia
[†] Deceased

JHEP07(2026)054